



**HAL**  
open science

## The shaping of a volcanic ridge in a tectonically active setting: The Pico-Faial Ridge in the Azores Triple Junction

Fernando Ornelas Marques, João Catalão, Christian Hübscher, Ana Cristina Goulart Costa, A. Hildenbrand, Hermann Zeyen, Paraskevi Nomikou, Elodie Lebas, Vittorio Zanon

### ► To cite this version:

Fernando Ornelas Marques, João Catalão, Christian Hübscher, Ana Cristina Goulart Costa, A. Hildenbrand, et al.. The shaping of a volcanic ridge in a tectonically active setting: The Pico-Faial Ridge in the Azores Triple Junction. *Geomorphology*, 2021, 378, pp.107612. 10.1016/j.geomorph.2021.107612 . hal-03398817

**HAL Id: hal-03398817**

**<https://hal.science/hal-03398817>**

Submitted on 23 Oct 2021

**HAL** is a multi-disciplinary open access archive for the deposit and dissemination of scientific research documents, whether they are published or not. The documents may come from teaching and research institutions in France or abroad, or from public or private research centers.

L'archive ouverte pluridisciplinaire **HAL**, est destinée au dépôt et à la diffusion de documents scientifiques de niveau recherche, publiés ou non, émanant des établissements d'enseignement et de recherche français ou étrangers, des laboratoires publics ou privés.



## 21 **Abstract**

22           The Pico-Faial ridge is a steep WNW-ESE volcanic ridge that has developed within the  
23 Nubia-Eurasia diffuse plate boundary, close to the Azores Triple Junction. The ridge comprises  
24 two islands, Pico and Faial, separated by a shallow (< 100 m depth) and narrow (< 8 km)  
25 channel. Despite some similarities, the two islands show contrasting features still deserving  
26 explanation: (1) meaning of GPS data; (2) meaning of palaeomagnetic data; (3) the island-scale  
27 Faial Graben does not have a counterpart in Pico; (4) both islands comprise a main central  
28 volcano each, but the one in Faial is symmetrical and the one in Pico is asymmetrical; (5) Pico  
29 shows evidence of at least two large-scale flank collapses, but none has been recognized so far in  
30 Faial. The new data reported here lead to the following probable answers: (1) the GPS data show  
31 much larger vertical and horizontal ground motions in Faial, which could be the result of recent  
32 volcanism and tectonics; (2) the cyclicity inferred from the paleomagnetic data in Pico could be  
33 related to inflation/deflation cycles that could have triggered the inferred flank collapses; (3) the  
34 Faial Graben ends abruptly at the eastern edge of the island, which we interpret as inhibited  
35 propagation to the east because of the load and stresses imposed by the nearby large Pico  
36 Volcano; (4) we attribute the asymmetry of the Pico Volcano to partial flank collapse  
37 recognizable in new offshore seismic profiles; (5) either the Faial island is actually  
38 gravitationally more stable, or there have been flank collapses not yet recognized. All these  
39 processes have concurred to shape the two islands and the ridge to their current morphology, but  
40 the current morphologies of Pico and Faial result mainly from three of these processes:  
41 volcanism, tectonics and large-scale landslides.

42

43 *Keywords:* Pico-Faial volcanic ridge; Azores Triple Junction; GPS ground motion; marine  
44 geophysical data; tectonics; large-scale flank collapse

45

## 46 **1. Introduction**

47 Volcanic ocean islands start as submarine seamounts that typically keep their conical or  
48 ridge-like morphology until the volcanic edifice reaches sea surface. During this seamount stage,  
49 the morphology of the volcanic edifice is mostly controlled by the volcanic activity and tectonics,  
50 unless gravitational instability leads to large-scale flank collapses. From the moment the seamount  
51 emerges (island stage), its morphology is controlled by several processes: volcanism (magma type,  
52 eruption type, output frequency and volume), erosion (small-scale – marine, meteoric and  
53 land/rock slides, and large-scale – flank collapses), tectonics (faults and earthquakes), isostasy  
54 (vertical island movements, depending mostly on loading/unloading and underplating), and  
55 eustasy (sea level changes). As a case study, we use the steep WNW-ESE Pico-Faial ridge that has  
56 developed within the Nubia-Eurasia diffuse plate boundary, because in such a geological setting  
57 tectonics add to volcanism in controlling the morphology of the islands. We conclude that the  
58 current morphologies of Pico and Faial result from three main processes: volcanism, tectonics and  
59 large-scale landslides.

60 The main motivation for this study is twofold: (1) to discern the main processes that concur  
61 to shape a volcanic island to its current morphology, and (2) understand why two islands so close  
62 to each other, making up the emerged portions of the same ridge, are morphologically so different.  
63 One is long and narrow, and the other more equidimensional; one is 2/3 made of fissural volcanism  
64 and 1/3 central volcanism, and the other is mostly dominated by a central volcano; one shows very  
65 little effects of tectonics (few and minor faults), and the other is dominated by an impressive island  
66 scale graben; one shows conspicuous signs of large-scale landsliding, and the other seems to be  
67 gravitationally stable, at least since 500 ka; one is the youngest in the Azores, and the other is five  
68 times older and the second oldest in the Azores Central Group; one was built by effusive volcanism  
69 but has the tallest volcano in the Azores, and the other has explosive volcanism (island blanketed  
70 with pumice) with a collapse caldera.

71 All the methods, results and processes presented and discussed in this work concur towards

72 a better understanding of the shaping of the ridge and islands on top of it. Geomorphology – the  
73 analysis and interpretation of digital elevation models (DEMs) representing the current topography  
74 helps with finding the main features that characterize each island; GPS – shows the current ground  
75 motion and how the islands are being deformed, and thus how it affects their shape; Marine  
76 Geophysics – the acquired data greatly helps in the recognition of large-scale landslides that  
77 rapidly and periodically shape the islands; Palaeomagnetism – it was first used in Silva et al. (2018)  
78 to analyse large-scale rotations within the two islands, and is here further used to help understand  
79 the shaping of the islands and the possible triggers of the recognised large-scale landslides that  
80 have shaped Pico; Geochemistry – helps to understand the differences in eruption style and,  
81 therefore, the morphological differences related to different types of eruption; Structural Geology,  
82 Tectonics and seismics – critical to the understanding of the position of volcanic vents, shape of  
83 eruption edifices, and overall shape of the ridge.

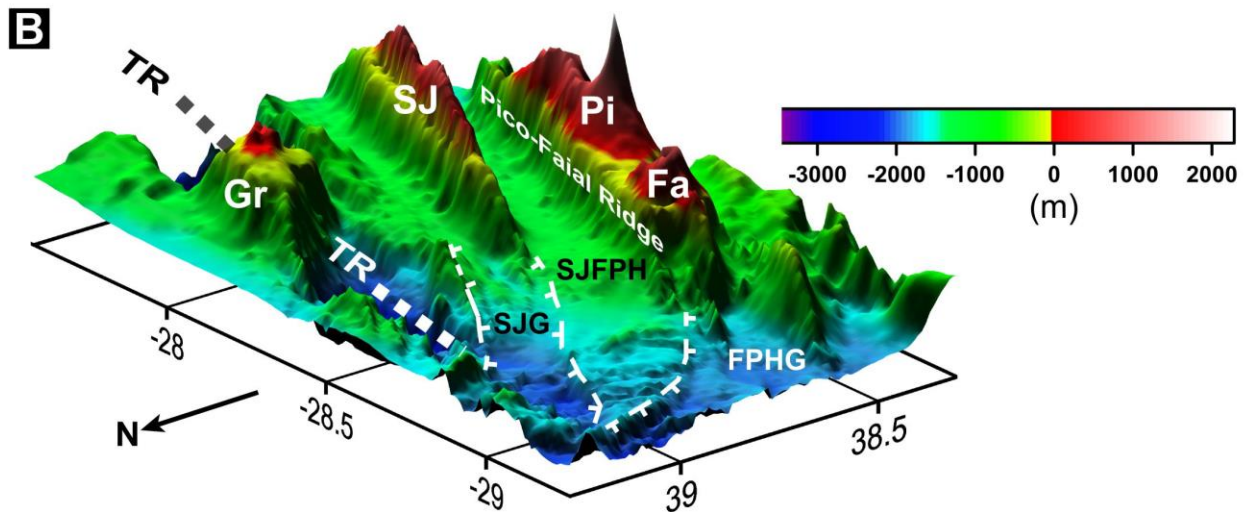
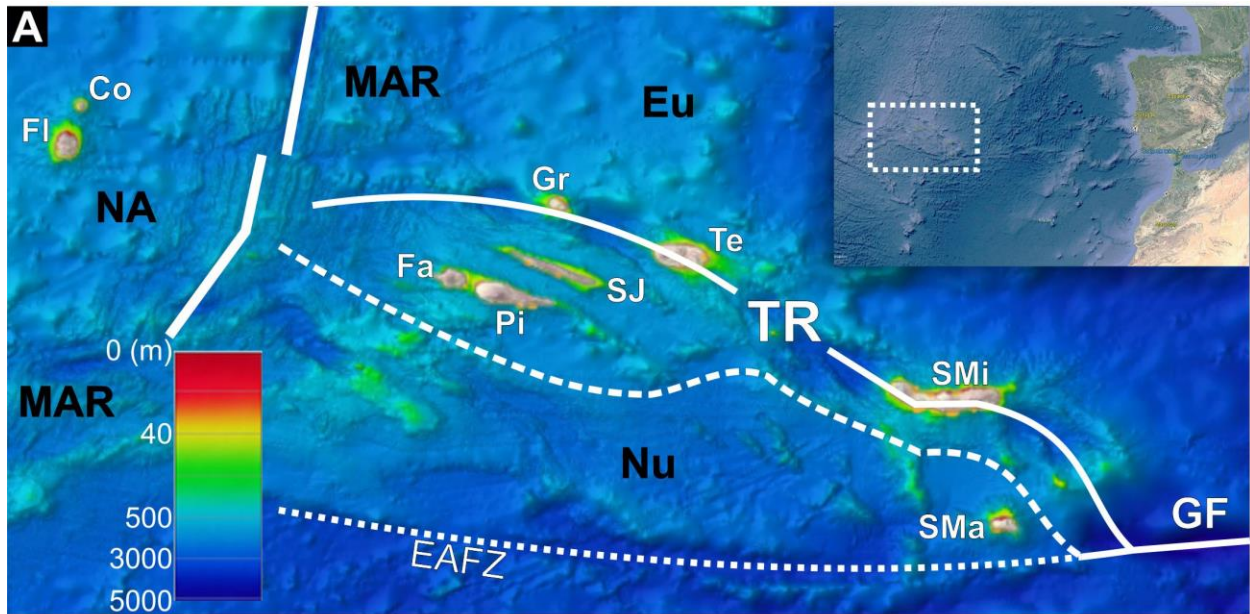
84 The Central Azores Group comprises the islands of Graciosa, Terceira, S. Jorge, Faial and  
85 Pico (Fig. 1), which formed during the last 2 Ma on top of an older oceanic crust (e.g. Calvert et  
86 al., 2007; Hildenbrand et al., 2008, 2012a; Sibrant et al., 2014; Costa et al., 2014, 2015; Marques  
87 et al., 2018). The Azores islands are volcanically active, except for Santa Maria Island, which is  
88 the oldest (Sibrant et al., 2015a; Ramalho et al., 2017; Marques et al., 2020). The most recent  
89 subaerial volcanism in the islands occurred in Faial, the Capelinhos eruption in 1957–1958  
90 (Machado et al., 1959, 1962; Zbyszewski and Veiga Ferreira, 1959).

91 The origin of the volcanism is still controversial: volatile-rich plume (e.g. Schilling et al.,  
92 1980; Bonatti, 1990; Métrich et al., 2014), or thermal mantle plume (e.g. Silveira et al., 2006;  
93 Gente et al., 2003; Madureira et al., 2005, 2011, 2014; Yang et al., 2006; Beier et al., 2010, 2012;  
94 Béguelin et al., 2017). Whatever the type of plume, the regional deformation seems to have  
95 controlled the distribution of the main volcanic outputs, with the formation of volcanic ridges  
96 striking along azimuth N110° in the diffuse boundary between the Eurasia and Nubia lithospheric

97 plates, and isolated islands inside the sinusoidal Terceira Rift (e.g. Borges et al., 2007; Marques et  
98 al., 2013, 2014a; Miranda et al., 2014; Hildenbrand et al., 2014; Marques et al., 2015) (Fig. 1a).  
99 The deformation in this diffuse plate boundary is mostly accommodated by several extensional  
100 structures trending WNW-ESE in a ca. 100 km wide area (Marques et al., 2013), which are from  
101 NE to SW (Fig. 1B): (1) the sinusoidal Terceira Rift, (2) the S. Jorge graben (Lourenço, 2007;  
102 Marques et al., 2018), (3) the S. Jorge-Pico/Faial horst, and (4) the Pico/Faial half-graben.

103         While the S. Jorge volcanic ridge developed apparently inside a graben, the S. Jorge  
104 Graben, the Pico-Faial ridge developed in great part on the master fault bounding the Faial/Pico  
105 half-graben in the north (Fig. 1). The sub-aerial growth of this ridge started ca. 850 ka ago in  
106 Faial (Hildenbrand et al., 2012a), which evolved by short periods of voluminous volcanic  
107 construction intercalated with longer periods of major erosion. The youngest mafic magmas (<11  
108 ka) on Faial have exclusively erupted along single rift zones and cover a smaller area, whereas  
109 the older volcanism was more widespread (Romer et al., 2018).

110         Sub-aerial Pico seems to be much younger than Faial (< 200 ka; Costa et al., 2014, 2015),  
111 and large-scale slumping and flank collapses have been recognised in both northern and southern  
112 flanks of the island (Hildenbrand et al., 2012b; Costa et al., 2014, 2015). The evolution of the  
113 steep Pico-Faial ridge appears intimately related to tectonic deformation, which may in part  
114 control the volcanic growth and repeated episodes of flank collapse (Woodhall, 1974; Costa et  
115 al., 2014, 2015) or large-scale slumping (Hildenbrand et al., 2012b).



116  
 117 *Figure 1. (A) Location of the Azores archipelago on the diffuse boundary between the North*  
 118 *America (NA), Eurasia (Eu) and Nubia (Nu) plates. Main active structures represented as thick*  
 119 *white lines (Mid-Atlantic Ridge – MAR, Terceira Rift – TR); southern limit of the diffuse Nu-Eu*  
 120 *plate boundary represented by dashed white line; and inactive structure as dotted white line*  
 121 *(East Azores Fracture Zone – EAFZ). (B) 3-D surface (viewed from NW and lighting from E) of*  
 122 *the sector that includes the WNW-ESE Pico (Pi)-Faial (Fa) volcanic ridge studied in this paper.*  
 123 *TR marked by thick dashed white line. The graben/horst structure SW of the TR is defined*  
 124 *according to Marques et al. (2013a, 2014a). SJG - S. Jorge Graben; SJFPH - S. Jorge/Pico-*  
 125 *Faial Horst; FPHG – Faial-Pico Half-Graben. Islands from W to E: FI – Flores; Co – Corvo;*  
 126 *Fa – Faial; Pi – Pico; Gr – Graciosa; SJ - S. Jorge; Te – Terceira; SMi – S. Miguel; SMA –*  
 127 *Santa Maria. Bathymetric data from EMODnet portal (<https://www.emodnet-bathymetry.eu/>).*  
 128

129 The integration of new and previous data on and around Pico and Faial allows discussing  
 130 the evolution of the ridge and the differences found in the two islands sitting on it. This study is  
 131 based on the analysis and interpretation of a high-resolution DEM, detailed stratigraphic and

132 structural observations and measurements, and GPS, marine geophysical, gravity anomaly and  
133 paleomagnetic data. In the frame of this study we addressed the following outstanding problems:

134 1. Why is there a concentration of volcanic output in two main conical volcanoes (Caldeira and  
135 Pico)? Why are they younger than the ridge itself? What has changed over time? Why do they  
136 have different ages, and the younger (Pico) is much larger and to the east (opposite to what is  
137 expected in a plate moving to the east)? At the scale of individual islands, it is apparent that  
138 volcanism youngs to the west, consistent with plate motion: in Faial, the oldest volcano (ca.  
139 850 ka) lies in the easternmost part of the island, the intermediate in the middle (Caldeira  
140 Volcano, > 130 ka), and the youngest at the western tip of the island (Capelinhos, erupted in  
141 the period 1957-1958); in Pico, the oldest volcano lies in the east (Topo Volcano, ca. 190 to  
142 125 ka) and the youngest in the west (Pico Volcano, < 60 ka). We use gravity anomaly data  
143 and the current knowledge about the ridge to address these problems.

144 2. Pico and Faial comprise a volcanic ridge but we can observe very few dykes, in great contrast  
145 to the nearby (< 18 km) S. Jorge volcanic ridge where dykes are pervasive and there is no  
146 central volcano (maybe it has existed in the earliest stage of S. Jorge). Why is that so? We use  
147 the gravity anomaly to address this problem.

148 3. What is the meaning of palaeomagnetic data? How can we explain the cyclic tilting? What are  
149 the effects of cyclic tilting on the stability of the island?

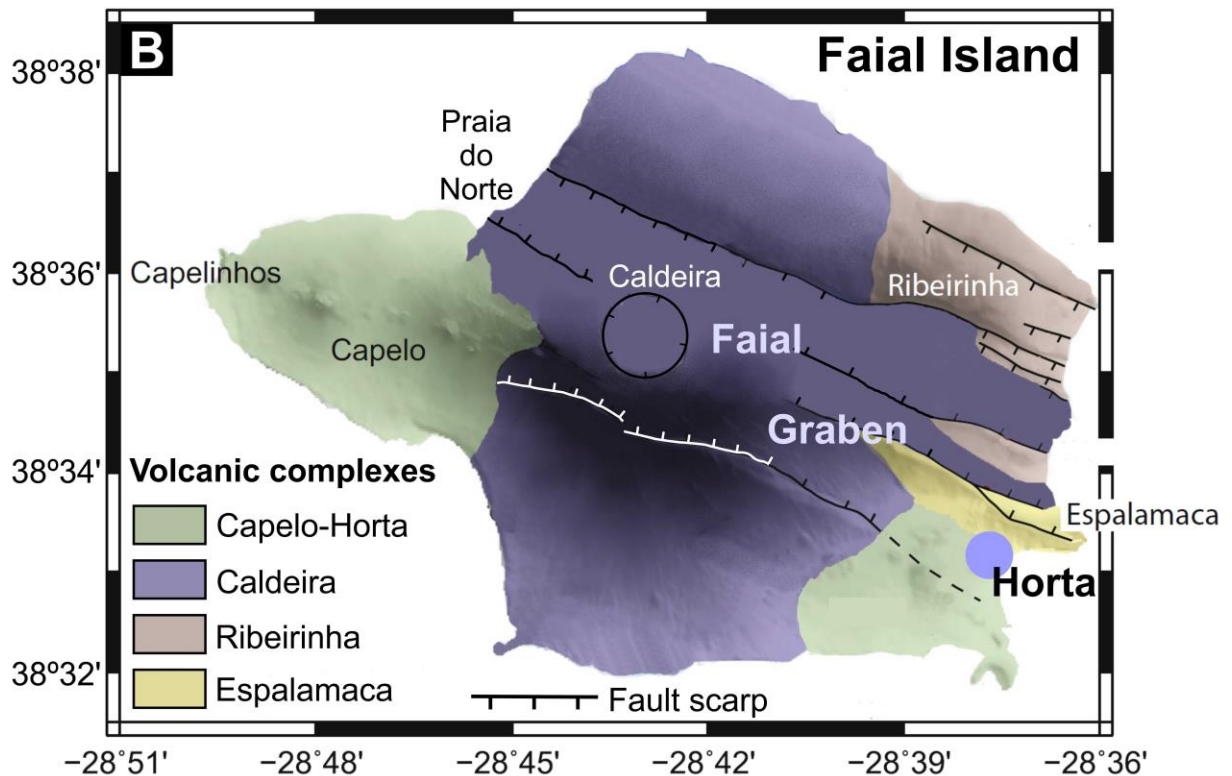
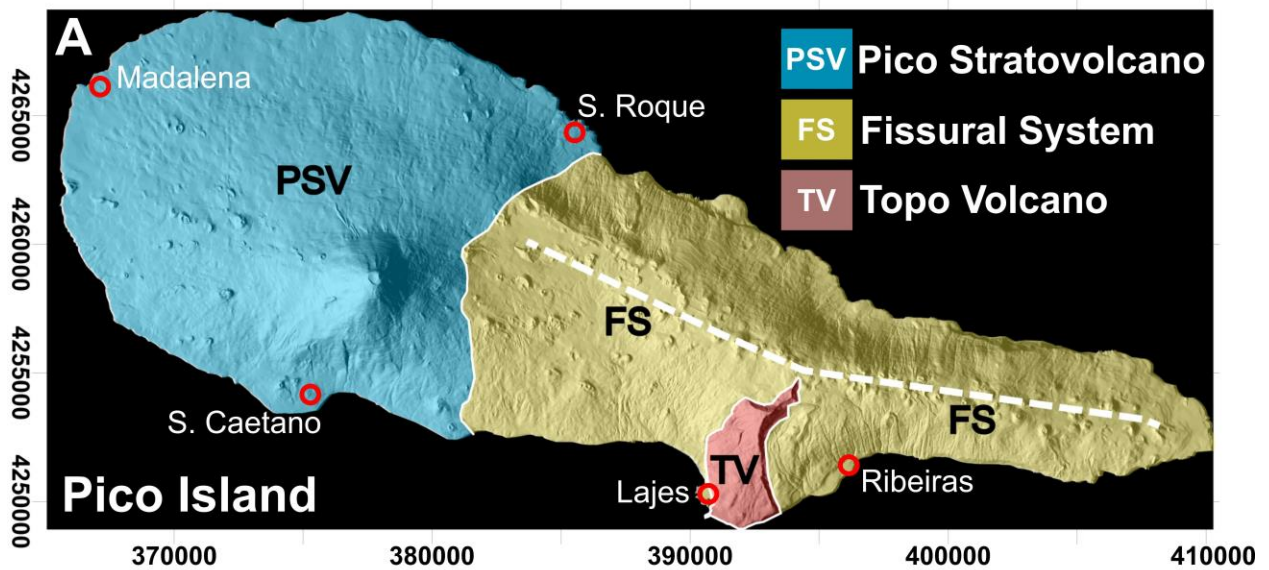
150 4. The island-scale Faial Graben does not currently have a counterpart in Pico: why? We use our  
151 knowledge about the ridge and mechanical concepts to address this problem.

152 5. Why is the Pico Volcano asymmetric? What is the meaning of the structures in the S. Caetano  
153 creek? We use marine geophysical data and the current knowledge about the ridge to address  
154 these problems.

155

156 **2. Geological background**

157           Some important tectonomagmatic trends have been recognized in the Azores east of the  
158 MAR axis. The N-S to NNE-SSW direction is a major regional trend parallel to the local  
159 orientation of the MAR axis (Fig. 1A). The WNW-ESE trend corresponds to the major  
160 horst/graben and volcanic ridge structures in central Azores (Fig. 1B). The NE-SW to ENE-  
161 WSW trend is a transform direction associated with the present Eu/Nu plate boundary (DeMets  
162 et al., 2010), and has been recognized by Marques et al. (2014b), Sibrant et al. (2014, 2015b,  
163 2016) and Zanon et al. (2020). These main trends can all be found in Pico: the dykes along the  
164 coastline range in strike between NNE-SSW and ENE-WSW (cf. Fig. 3 in Costa et al., 2015);  
165 the sea cliff and the marine platform that limit the sub-aerial remnants of Topo Volcano to the E  
166 are oriented ENE-WSW (Fig. 2); Pico is elongated WNW-ESE, and the Caldeira (Faial), Pico  
167 and Topo volcanoes are aligned along the same trend (Fig. 2). In Faial, the most conspicuous  
168 trend is that of the island-scale graben, the WNW-ESE Faial Graben, and the alignment of young  
169 strombolian cones (Fig. 2).



170  
171  
172  
173  
174  
175

Figure 2. Shaded relief of the 10 m resolution DEM of Pico Island overlain by simplified geological map (A – modified after Madeira, 1998), and shaded relief of the 50 m resolution DEM of Faial Island overlain by simplified geological map (B – modified after Silva et al., 2018).

176 Pico Island comprises three main volcanic complexes, from older to younger (Fig. 2A):  
177 the Topo volcanic complex in SE Pico, the Fissural Complex in central and eastern Pico, and the  
178 Pico Volcano (peaking at 2351 m altitude), which makes up the western half of the island (e.g.

179 Zbyszewski et al., 1963; Forjaz, 1966; Woodhall, 1974; Madeira, 1998; Nunes, 1999; França,  
180 2000; Madeira and Brum da Silveira, 2003; França et al., 2006). The Topo complex is partly  
181 exposed on Pico's SE flank and was dated between  $186 \pm 5$  and  $125 \pm 4$  ka (Costa et al., 2014,  
182 2015). Remnants of this early sub-aerial volcano have been unconformably covered by the sub-  
183 aerial Fissural Complex. The latest stages of island growth comprise the development of the  
184 Fissural Complex and the Pico Volcano, which have been active through the Holocene up to  
185 historical times. The Pico Volcano grew in western Pico, at least since ca. 57 ka. The Topo  
186 Volcano was mostly destroyed by a N-directed flank collapse between ca. 125 and 70 ka (Costa  
187 et al., 2014). In the south, the collapse structure was composite, with an early flank collapse  
188 (between ca. 125 and 70 ka), followed by a remnant slump complex in the western part of the  
189 collapse that seems to be still active (Hildenbrand et al., 2012b; Costa et al., 2015). Following  
190 the collapses, the scars were partially filled by lavas erupted from volcanic cones on the  
191 topographically higher Fissural Complex.

192 Isotope dating in Faial (Hildenbrand et al., 2012a) showed inconsistencies in the  
193 geological mapping (Chovelon, 1982; Serralheiro et al., 1989; Madeira, 1998; Pacheco, 2001;  
194 Tripanera et al., 2014), and served as basis to a revised stratigraphy, which is from older to  
195 younger (Fig. 2B): (1) a ca. 850 ka first sub-aerial volcanic complex, the Lower Volcanic  
196 Complex, whose remnants outcrop in eastern Faial, immediately north of Horta city and along  
197 the scarp of a main normal fault (Espalamaca fault). (2) A ca. 360 ka volcanic complex, the  
198 Intermediate Volcanic Complex, whose remnants outcrop on the NE quadrant of Faial around  
199 the Ribeirinha village. (3) The Upper Volcanic Complex, mostly composed of the Caldeira  
200 Volcano and built on the remnants of the Lower and Intermediate Volcanic Complexes. The  
201 Caldeira Volcano rapidly grew during a main phase of activity between ca. 130 and 115 ka, but  
202 its volcanic and sedimentary products have covered the island till the present, which include  
203 widespread trachytic pumice deposits produced by recent explosive activity of the Caldeira

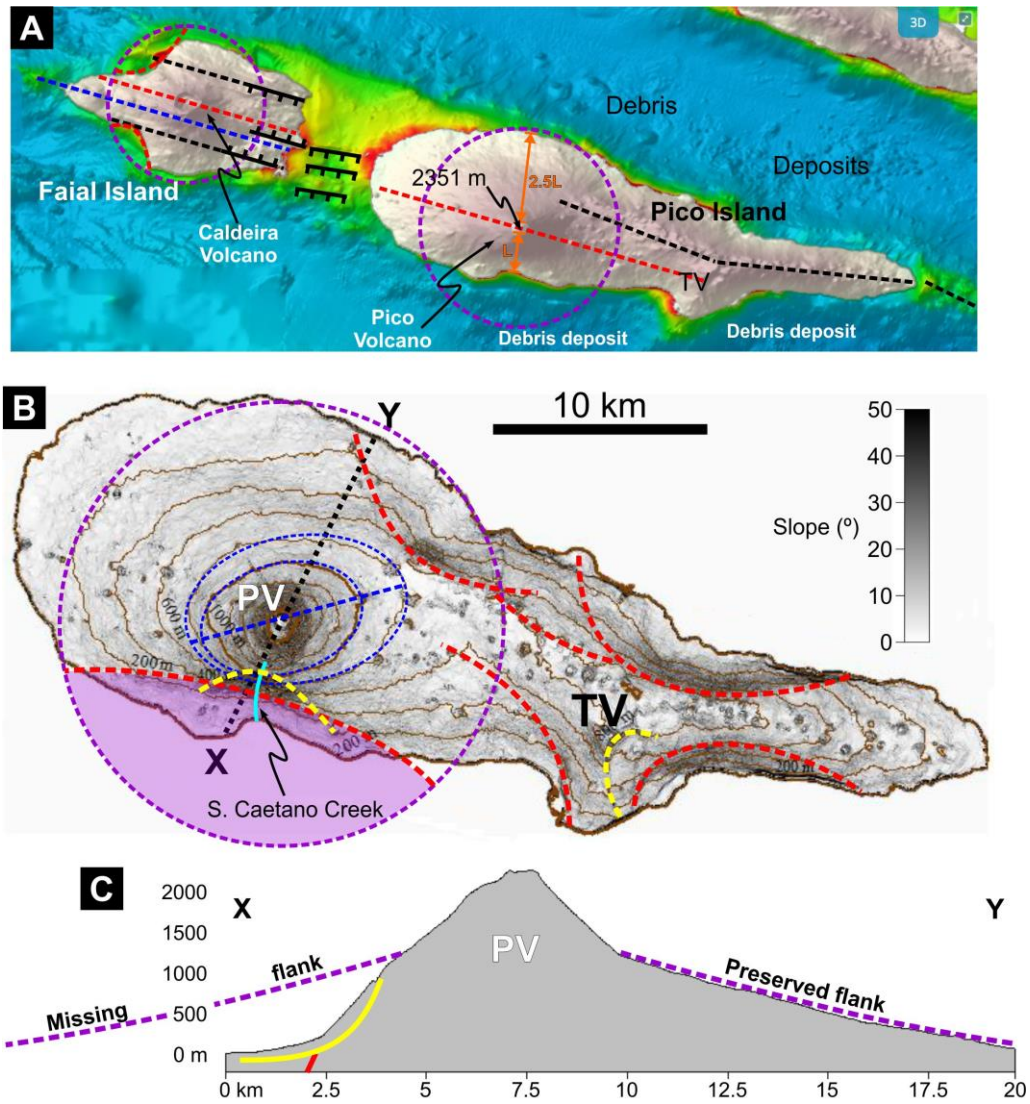
204 Volcano over the last 16 ka (Pacheco, 2001). Basaltic units in the SE quadrant of Faial (Horta)  
205 and west of the Caldeira Volcano (“Capelo”) comprise an important part of the Upper Volcanic  
206 Complex. The Horta volcanism, located in the SE corner of the island, is characterized by a  
207 series of small scoria cones and associated basaltic lava flows. The Capelo volcanism  
208 corresponds to the most recent volcanic activity in the ridge, which formed a peninsula in the  
209 westernmost part of Faial, thus recently adding to the volume of the island during the 1957–1958  
210 eruption. The Horta and Capelo volcanic products have been erupted during the last 10 ka  
211 (Madeira et al., 1995), and are morphologically characterized by a series of WNW-ESE aligned  
212 Strombolian cones that stretch the island towards the Capelinhos Volcano. The recent eruptive  
213 history of Faial has been dated by radiocarbon on charcoal fragments collected in pyroclastic  
214 deposits and/or palaeosoils (e.g. Madeira et al., 1995; Pacheco, 2001; Chiara et al., 2014). All  
215 these volcanic units have been affected by an island-scale WNW-ESE trending graben, the Faial  
216 Graben, which is still active (e.g. Marques et al., 2014b).

217

### 218 **3. Methods and results**

219 We used several methods and datasets to accomplish the objectives of this work. Some  
220 are new and make up the novel contribution (topography analysis, GPS, field work, structural  
221 and tectonic analysis, and marine geophysics), and some are borrowed from the literature  
222 (palaeomagnetism and petrology/geochemistry). Details of the methods used to accomplish the  
223 results described below can be found in the Supplementary material section, and details of the  
224 remaining methods can be found in the cited literature.

225



226  
 227 *Figure 3. Interpreted shaded relief image (A) and slope map (B), and topographic profile across*  
 228 *the Pico Volcano (C – marked X-Y in B). Red dashed lines –scars of main flank collapses. Yellow*  
 229 *dashed lines – headwalls of inferred slumps. Purple dashed circles – inferred original shape of*  
 230 *the base of the main Pico and Caldeira volcanoes. Purple shaded area in B – inferred missing*  
 231 *flank of Pico Volcano. Dashed blue ellipses superposed on the contour lines to highlight the*  
 232 *elliptical character of the Pico cone, with the axis of the ellipse (blue dashed line) trending ENE-*  
 233 *WSW. PSV – Pico Volcano. TV – Topo Volcano. Background image in A from EMODnet portal*  
 234 *(<https://www.emodnet-bathymetry.eu/>).*  
 235

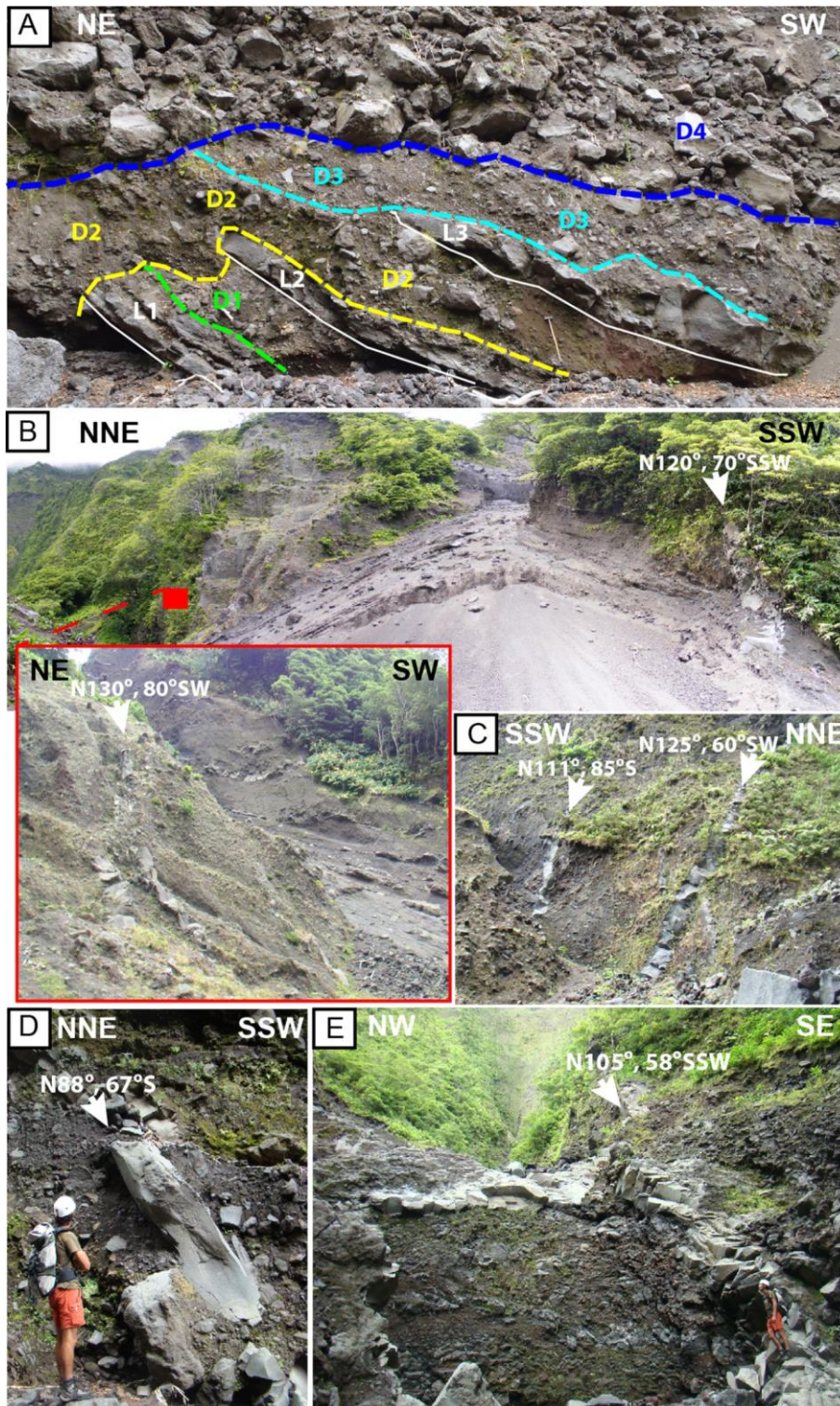
### 236 3.1. Geomorphological analysis

237 Subaerial Pico is elongated along the WNW-ESE direction, and is continued in the east  
 238 by a NW-SE submarine ridge (Fig. 3A). Pico has a maximum length of ca. 46 km and maximum  
 239 width of ca. 16 km, and peaks at 2,351 m altitude. Its overall linear morphology is interrupted by

240 two central volcanoes, one older and mostly destroyed, the Topo Volcano, and the other younger  
241 and mostly preserved, the Pico Volcano. Constructional slopes can reach more than 15°,  
242 especially in the upper half of the Pico Volcano. Much steeper slopes are locally observed on the  
243 island (Fig. 3), which correspond to impressive sub-vertical cliffs that cut the volcanic  
244 successions, and to scarps related to mass-wasting/faulting. These sub-aerial scarps are often  
245 blanketed by more recent volcanic deposits.

246         The sub-aerial Fissural Complex changes trend from ca. E-W in the E to WNW-ESE in  
247 the W, with inflection point near the Topo Volcano (Fig. 3A). The axis of the Fissural Complex  
248 is well-defined and narrow to the E of the Topo Volcano, and becomes wider towards the Pico  
249 Volcano. The northern flank of the Fissural Complex presents two steep scarps, and the southern  
250 flank one conspicuous scarp on its eastern half, all of them with headwalls trending parallel to  
251 the ridge (Fig. 3B). The topographic expression of all these scarps is obscured by volcanic  
252 products erupted from the axis of the Fissural Complex and from cones located on the scarp, and  
253 by the eastern flank of the Pico Volcano.

254         The western half of the island is dominated by the Pico Volcano, with quite an  
255 asymmetrical and elliptical conical shape (Fig. 3B): a larger, well-preserved half elliptical cone  
256 in the northern flank, in contrast to a much smaller southern flank where two scarps can be  
257 distinguished: one wider and closer to the sea, and the other narrower and cut by a deep creek  
258 (the S. Caetano creek). If the original Pico Volcano were a circular cone, then a great portion of  
259 its southern flank is missing, as drawn in Figs. 3B and C. The centre of the Pico Volcano is  
260 located S of the longitudinal axis of the island (Fig. 3A) and defines an alignment with the Topo  
261 Volcano that is parallel to the island axis.



262

263 *Figure 4. Photographs taken inside the S. Caetano canyon (order according to upslope*  
 264 *observations). (A) Lava flows intercalated with sedimentary deposits. (B) Thick small grained*  
 265 *volcaniclastic (pyroclastic) sequence with some thin lava flows intercalated and cut by steeply*  
 266 *dipping dykes. Zoom in: view of the dykes located near the red square. (C) Small-grained*  
 267 *volcaniclastic sequence intruded by en échelon dykes. (D) and (E) Metre thick dykes steeply*  
 268 *dipping towards downslope, cutting the sequence of lava flows and volcano-sedimentary*  
 269 *material. The dykes and their orientations are indicated by white arrows.*

270 The morphology of Faial is dominated by three main structures (Fig. 3A): the circular  
271 conical Caldeira Volcano with a deep central collapse crater; the island-scale graben known as  
272 the Faial Graben (Hildenbrand et al., 2012a); and aligned Strombolian cones, especially those  
273 making up the Capelo peninsula that stretches the island to the west. Two possible small-scale  
274 collapse scars may be interpreted in western Faial (Fig. 3A). Noticeably, the prominent Faial  
275 Graben does not extend east into the Pico-Faial channel and Pico Island (Fig. 3A).

276

### 277 3.2. Field data

278 New fieldwork on Pico was focused on the scarp that affects the southern flank of the  
279 Pico Volcano, and detailed observations were made along the S. Caetano canyon (Fig. 4). From  
280 downstream to upstream, we observed:

- 281 1. Lava flows dipping downslope, i.e. to the south (*L1* to *L3*, Fig. 4A), intercalated with  
282 sedimentary deposits (*D1* to *D3*, Fig. 4A), all overlain by a coarse (boulders) talus deposit  
283 several meters thick (*D4*, Fig. 4A). Though there are coarse deposits related to the current  
284 canyon erosion, we observed that the metre-thick deposits are overlain by, at least, one lava  
285 flow.
- 286 2. Several meters thick sequence of volcano-sedimentary material intercalated with lava flows,  
287 and intruded by dykes that strike N88-130°, mostly steeply dipping downstream (examples in  
288 Figs. 4B to 4E). The thickness of the dykes ranges between decimetres and metres. The  
289 thinner ones are sometimes disposed *en échelon*, with average strike of N120° azimuth and  
290 dip of 50-65° towards the SSW (Fig. 4C).

291 The stratigraphic relationship between the sequences described in 1 and 2 is not clear.  
292 However, the coarse talus deposit *D4* in Fig. 4A seems to unconformably cover also the  
293 downslope limit of the sequence described in 2 (Fig. 4B).

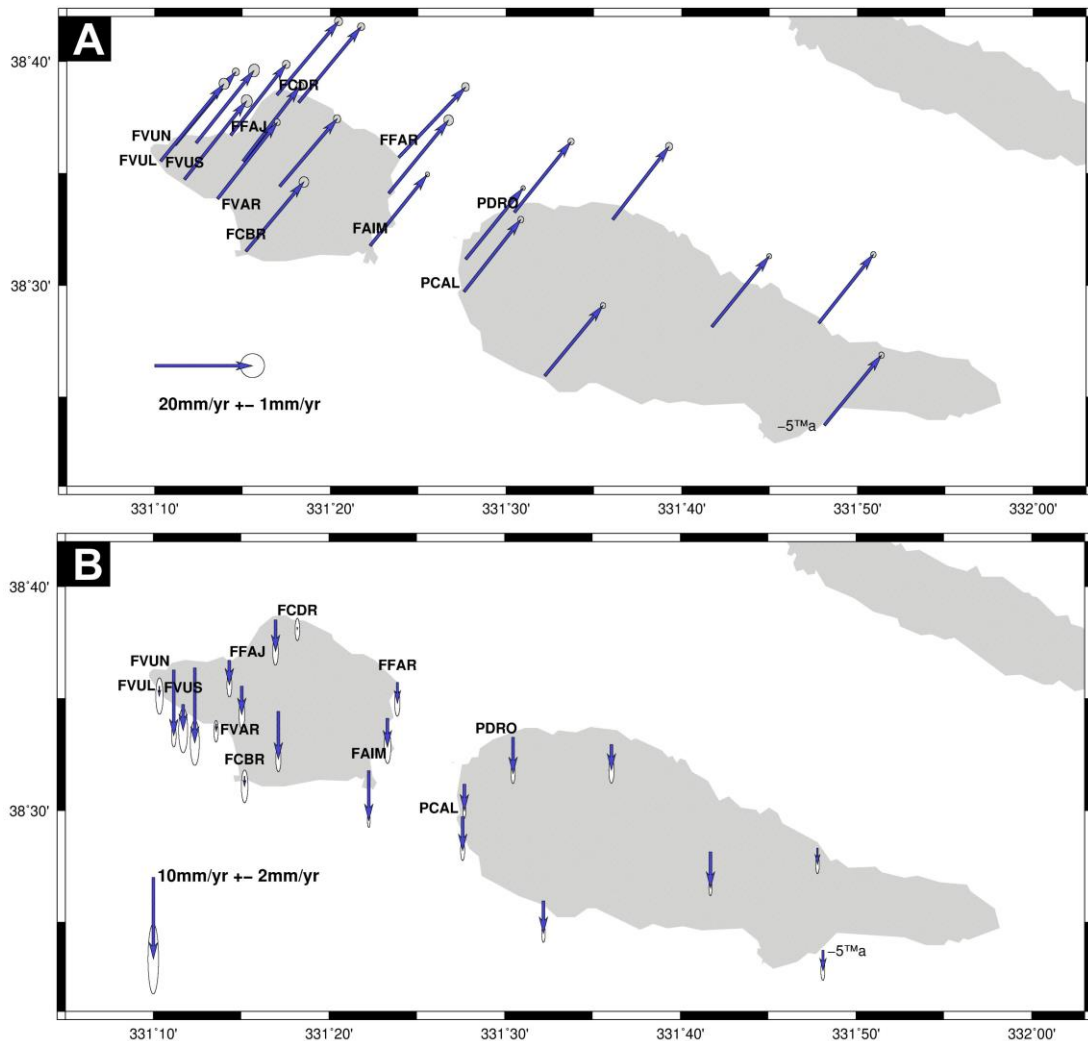
294 We did not observe an unconformity surface that could correspond to the failure surface

295 of the S. Caetano scar. Unfortunately, the volcanic deposits observed did not present the  
296 conditions favourable for K-Ar dating, because the observed lava flows are extremely vesicular.

297

### 298 3.3. GPS velocities

299 Figure 5 shows the GPS site velocities for Faial and Pico islands with respect to ITRF-14  
300 reference frame. Faial and Pico islands are moving northeast with a mean velocity of 24 mm/yr  
301 and moving down about 4 mm/yr on average. On western Faial, two stations have been moving  
302 down consistently in the analysed period, with a higher than average rate of about 10 mm/yr (2.5  
303 times the average).



304

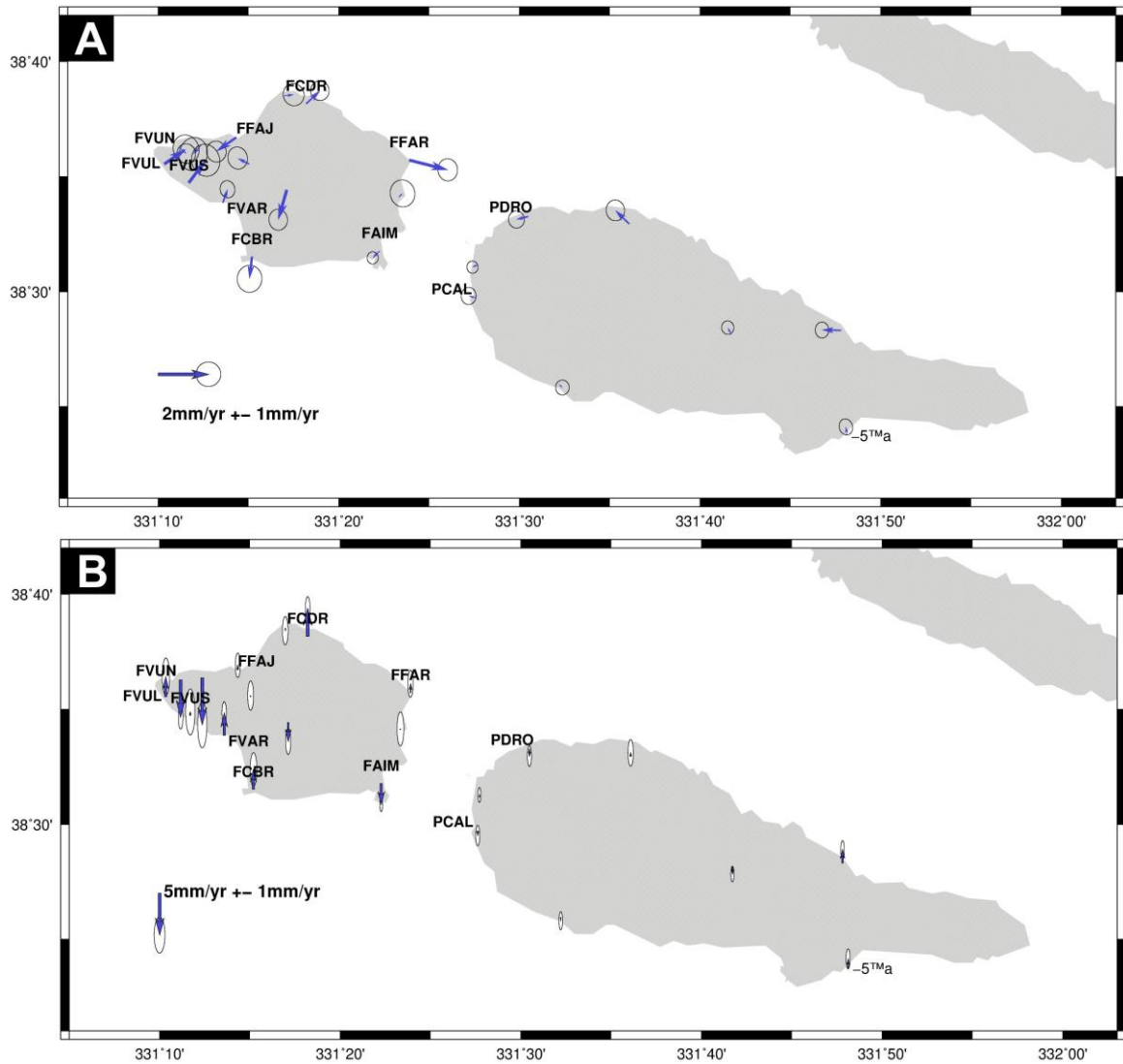
305 *Figure 5. Horizontal (A) and vertical (B) velocities of GPS stations used for the analysis. All*  
306 *velocities are relative to ITRF-14.*

307

308           The estimated horizontal surface velocities were assumed to be representative of two  
309 main processes: a rigid body motion associated with the regional plate tectonics, and a residual  
310 displacement associated with the intra-island deformation. The rigid body motion was estimated  
311 using the Euler vector notation. The three vector components were computed in the least squares  
312 sense using the estimated GPS velocities and further used to compute the rigid body motion and  
313 the velocity residuals. Using these parameters, the velocity of the rigid body motion of Faial and  
314 Pico Islands is easting 13.7 mm/yr, and northing 15.6 mm/yr. The residuals between the  
315 velocities obtained for each station and the rigid body motion are the consequence of local  
316 variations of the strain field and are within 2 mm/yr for the residual horizontal velocity. We plot  
317 the horizontal residuals in Fig. 6, together with the 95% confidence error ellipses for each  
318 station.

319           The residual of the horizontal velocity shows that: a) there is no evidence of internal  
320 deformation in Pico island, in contrast to what is shown by InSAR (Hildenbrand et al., 2012b);  
321 b) the eastern half of Faial is similar to Pico (except for station FFAR); and c) the sites on the  
322 south of westernmost Faial are moving faster than sites on the north, showing a centripetal  
323 distribution. Still on western Faial, sites FVUN and FPDN show a consistent downward  
324 movement of up to 10 mm/yr.

325



326 *Figure 6. Residual horizontal (A) and vertical (B) velocities obtained by extracting rigid-body*  
 327 *motion from the velocities of the network. Error ellipses correspond to 95% confidence. Arrows*  
 328 *pointing north or south mean upward or downward motion, respectively. This means that, in the*  
 329 *Capelo region (inset with zoomed westernmost Faial in B), the southern coast is moving*  
 330 *upwards and slow, and the northern coast is moving down and faster.*  
 331  
 332

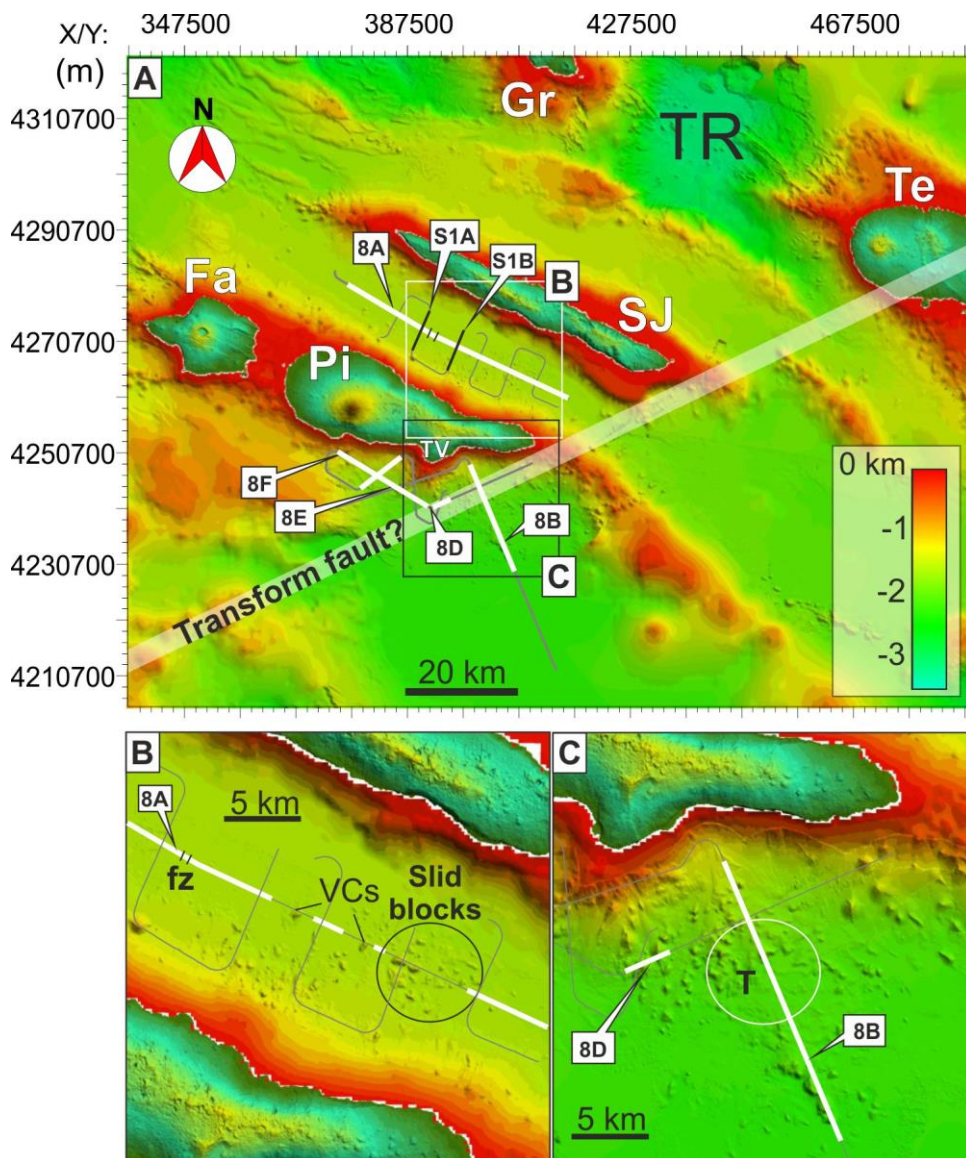
### 334 3.4. Marine geophysical data

335 We discuss the marine record of downslope mass transport by means of the bathymetry  
 336 and four seismic profiles (Figs. 7 and 8). The bathymetry shows the islands, the fringing shelves  
 337 and the volcanic ridges in detail. SE of Pico, the submarine Pico ridge changes its strike from  
 338 116° to 133° in azimuth. Submarine volcanic cones (VCs) concentrate in the channel between  
 339 SE Pico and S. Jorge as well as south of Topo Volcano.

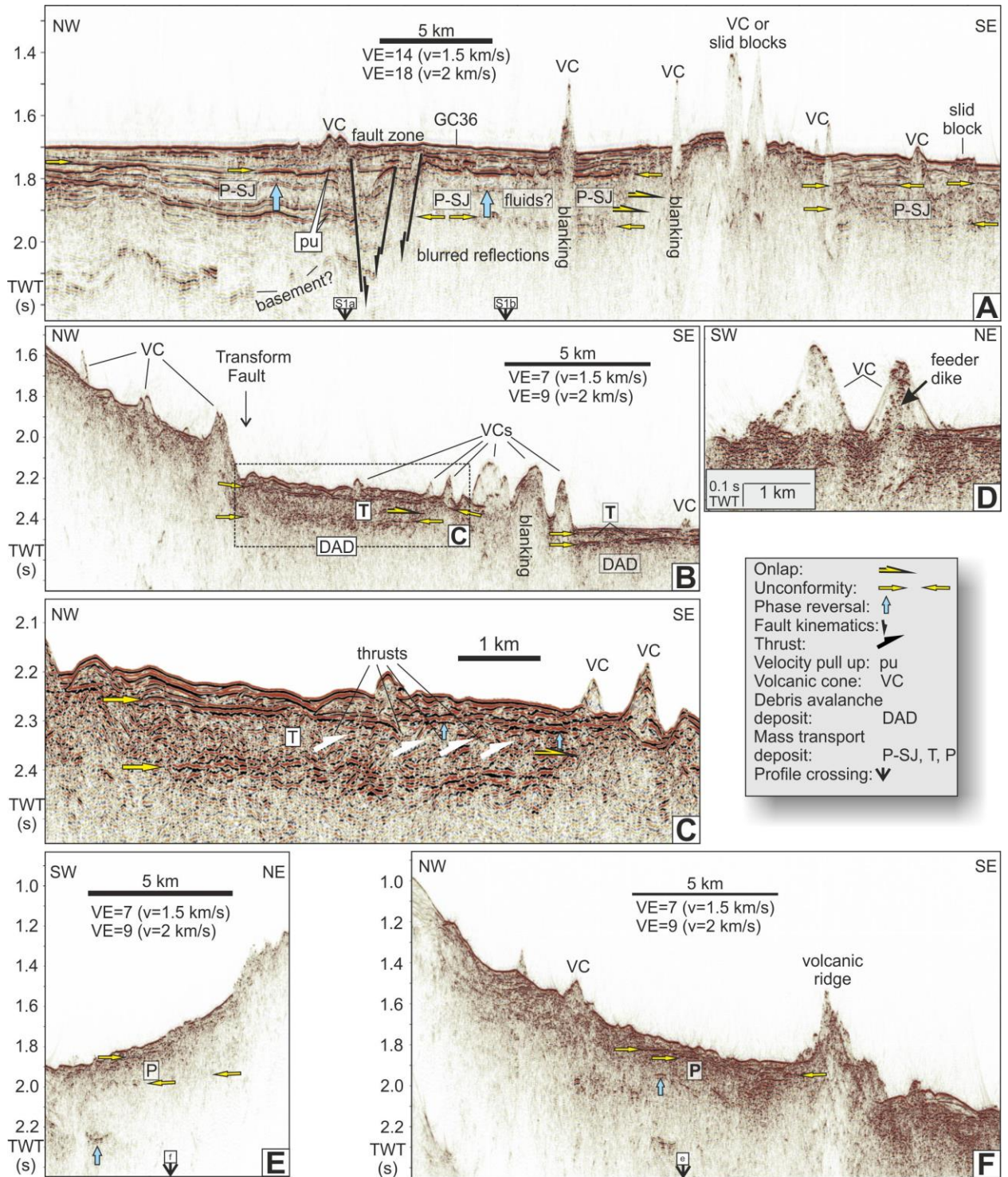
340           Along the channel between the islands of Pico and S. Jorge, the 42 km long seismic  
341 profile elucidates the upper 400-500 ms TWT, which corresponds to 300 to 500 m if average  
342 velocities between 1.5 km/s and 2 km/s are assumed (Fig. 8A). A fault zone that propagates up to  
343 the seafloor and of unknown strike divides the profile into the WNW segment with rather good  
344 signal penetration, and the ESE segment with reduced penetration and blurred reflections (Fig.  
345 8A). In the WNW segment, a strong reflection package of positive polarity at 400-500 ms  
346 beneath the sea floor represents the acoustic basement, which is not seen ESE of the fault zone.  
347 Except for a 5 km long area in the ESE part of the profile, two unconformities can be traced  
348 along the profile, covering a TWT interval of ca. 60-150 ms TWT, which is labelled Unit P-SJ.  
349 The top of this unit is visible ca. 50 - 100 m below the seabed. Internal reflections of Unit P-SJ  
350 are only vaguely visible ESE of the fault zone, and few of the internal reflections are phase  
351 reversed. To the ESE, Unit P-SJ overlies a ca. 5 km wide elevated zone, which is seismically  
352 opaque except for the upmost 30-40 ms TWT. The multibeam and seismic data show that the  
353 eastern part of the profile crosses a field of large blocks. Some of them are cone shaped and  
354 likely represent volcanic cones. Yet, some of the blocks, which are located offshore a major  
355 embayment on Pico's northern flank, reveal an irregular topography, which is not typical of  
356 volcanic cones. These features most likely represent slid blocks in a large-scale landslide. On the  
357 seismic line (Fig. 8A) it becomes more apparent that most of the irregularly shaped blocks  
358 represent slid blocks covered by a thin sediment veneer. Sparker profiles (Fig. S1) indicate that  
359 unit P-SJ was transported downslope Pico.

360           Offshore and south of the ancient Topo Volcano, the ca. 22 km long and NW-SE striking  
361 seismic reflection profile images the marine archive of mass transport processes (Fig. 8B). It  
362 covers Pico's lower slope and the adjacent archipelago's apron south of Pico. The signal  
363 penetration is limited to about 200 ms TWT. The transition from the lower slope to the plateau is  
364 rather abrupt. The profile crosses several VCs. Two approximately horizontal unconformities

365 cover a time interval of ca. 100 ms TWT directly in front of the lower slope and ca. 50 ms TWT  
 366 SE of a VC complex. Assuming interval velocities between 1.5 km/s and 2 km/s, the thickness  
 367 varies between 40 and 100 m. The deposits in between, labelled Unit T, onlap the lower, buried  
 368 part of a VC. The upper bounding unconformity reveals a polarity change along its southern part  
 369 (Fig. 8C). The internal strata are folded and thrust. A short profile illuminates the internal  
 370 architecture of VCs, which comprises strong reflection patches beneath the summit and outward  
 371 dipping strata around them (Fig. 8D).



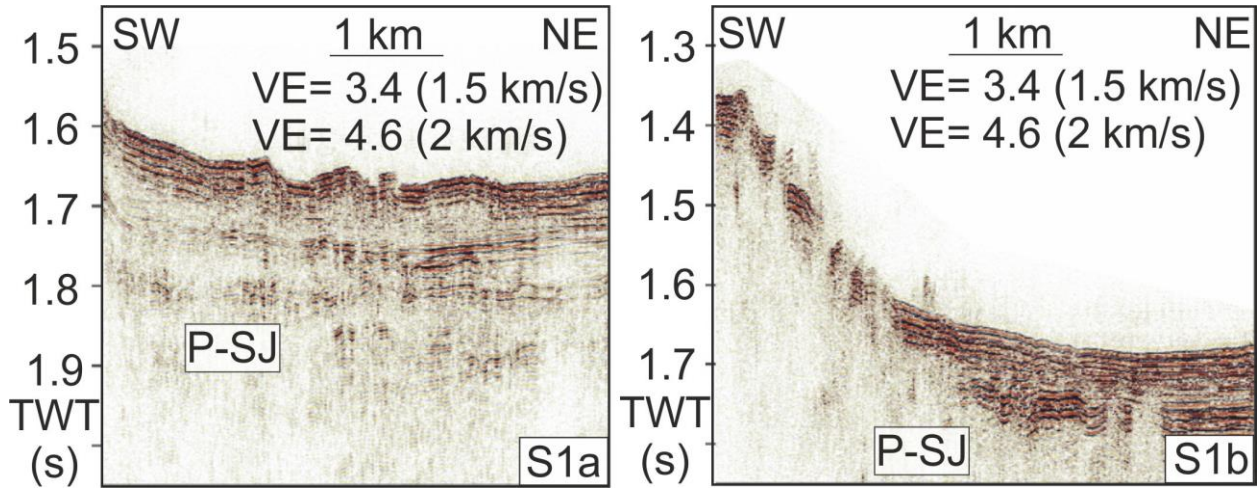
372  
 373 *Figure 7. A – overview map. B – blow-up of study area between Pico and S. Jorge. C – survey*  
 374 *area in southeastern Pico. The circle in C is used to estimate the volume of unit T. White lines*  
 375 *mark the location of seismic profiles shown in Fig. 8. fz: fault zone; TV: Topo Volcano. Other*  
 376 *symbols as in Fig. 1.*  
 377



378  
 379  
 380 *Figure 8: Seismic profiles. For locations see Fig. 7. GC36: Gravity core 36 as discussed in*  
 381 *Schmidt et al., 2020. VE: vertical exaggeration according to given velocity v. VC: volcanic cone.*  
 382

383  
 384  
 385

386 An 8-9 km long profile south of central Pico shows mainly chaotic reflections that  
 387 downlap a unit between two parallel, horizontal unconformities (Fig. 8E, F). The TWT interval  
 388 for this unit, also labelled “P”, is ca. 120 ms (90-120 m). Here too, the top of unit “P” is  
 389 horizontal in places.



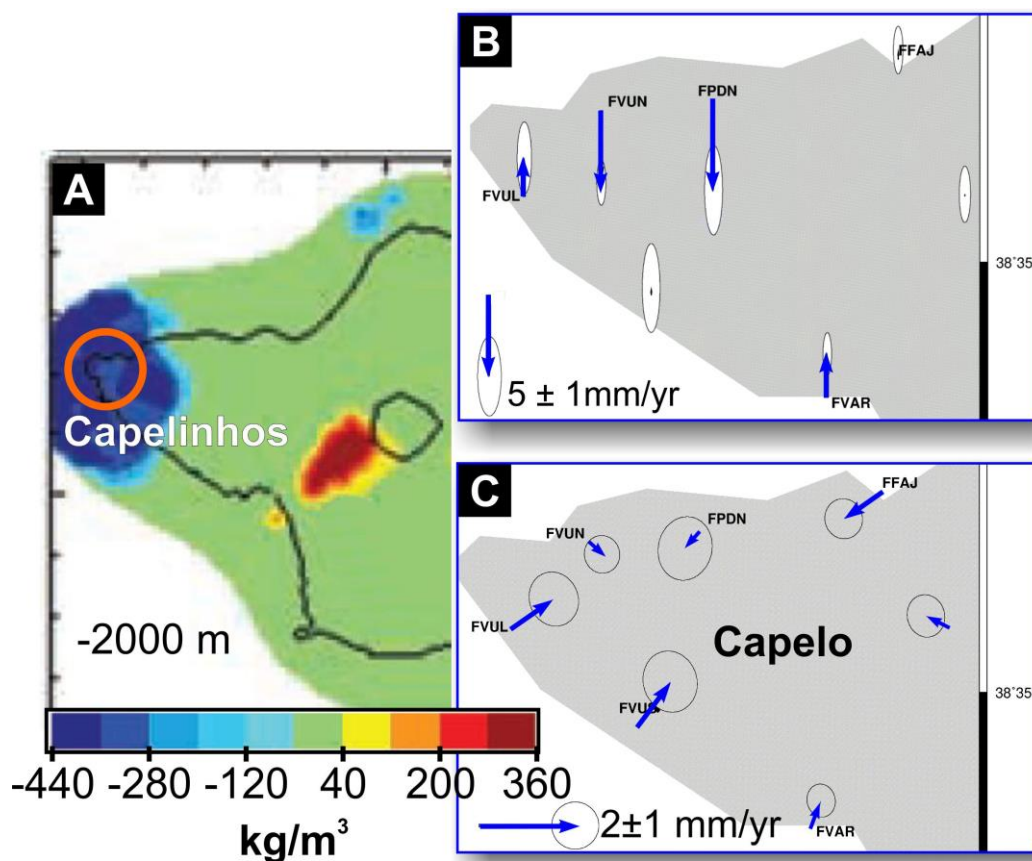
391 *Figure S1. Sparker profiles. For locations see Fig. 7. VE: vertical exaggeration according to*  
 392 *given velocity given in brackets. Meaning of symbols as in Fig. 8.*

#### 394 4. Discussion

##### 395 4.1. GPS and gravity data

396 In Faial, two regions deserve special attention: Ribeirinha at the NE tip of the island, and  
 397 Capelo in westernmost Faial (Figs. 5 and 6). At Ribeirinha (GPS station FFAR; Fig. 6A), the  
 398 residual horizontal velocity is anomalous regarding magnitude and direction, meaning that this  
 399 station is moving to the east instead of the northeast (relative to ITRF14; Fig. 5A), and faster  
 400 than the rest of the island. This cannot be attributed to creep on a slope because the station is  
 401 following the vertical motion of the island (zero vertical residual velocity; Fig. 6A). Our  
 402 interpretation is that NE Faial is being affected by the motion in the faults discussed in Marques  
 403 et al. (2014b). In westernmost Faial, the distribution and magnitude of GPS velocities may have  
 404 four kinds of explanations: mechanical (flexural effect), tectonic (normal fault), magmatic  
 405 (magma motion), or tectonomagmatic (tectonic triggered by magma motion). The northern coast

406 is moving downward and fast (Fig. 9B), which could be the consequence of the eruption of  
 407 Capelinhos in 1957-58, because the contraction of cooling magma/rock could be responsible for  
 408 the anomalous downward velocity (ca. 2.5 times the average on the island). However, the  
 409 southern coast is moving upward and slowly, and the horizontal residual velocity (Fig. 9C) is  
 410 centripetal, i.e. the stations on the north coast are moving south, and the stations on the south  
 411 coast are moving north. Again, one possible interpretation is contraction of the hot magma/rock  
 412 for the centripetal velocities, but contraction cannot explain the upward velocity in the south. A  
 413 possible explanation for this upward velocity could be liquid magma moving in the vertical  
 414 feeder cylinder (convection with upward motion in the south and downward in the north).  
 415 However, there are two problems with these interpretations: (1) the GPS stations are offset to the  
 416 east from the gravity anomaly, and (2) we do not know if contraction by cooling is a viable  
 417 mechanism to explain the vertical velocities. To test this second hypothesis, we calculated the  
 418 effects of contraction on the vertical velocity.



419

420 *Figure 9. Gravity anomaly (A) and residual vertical (B) and horizontal (C) GPS velocity maps.*  
421 *The negative gravity anomaly (blue spot) below Capelinhos (orange circle in A) can be*  
422 *interpreted as hot magma/rock with lower density. Arrows pointing north or south in B mean*  
423 *upward and downward motion, respectively. This means that, in the Capelo region (insets B and*  
424 *C), the southern coast is moving upwards and slowly, and the northern coast is moving*  
425 *downward and faster. Map of gravity anomaly in A cropped and adapted from Fig. 11 in*  
426 *Camacho et al. (2007).*  
427

428 Although the reasons for the higher downward velocities at Capelo are unclear, their  
429 proximity to the 1957/58 eruption that added 1.5 km<sup>2</sup> to western Faial suggests a volcanic origin  
430 for the anomalous GPS velocities (Catalão et al., 2006; Marques et al., 2013). Therefore, we  
431 tested this hypothesis by following the results of gravity inversion published by Camacho et al.  
432 (2007) and performing preliminary and simplified modelling of an intrusion between 1 and 4 km  
433 depth, with an initial temperature of 1250 °C, allowing for a complete melting of the rock. We  
434 then let this intrusion cool down and densify, using a thermal expansion coefficient of  $3.5 \times 10^{-5}$   
435 K<sup>-1</sup> for the solid rock, observing the local isostatic effect of the density increase and thus the  
436 evolution of the subsidence rate. The 1-D model reduces to a certain degree the cooling rate with  
437 respect to a 3-D model; however, since the width of the gravimetric anomaly, and thus the  
438 supposed width of the intrusion, is far larger than its depth, the effect should not be very strong.

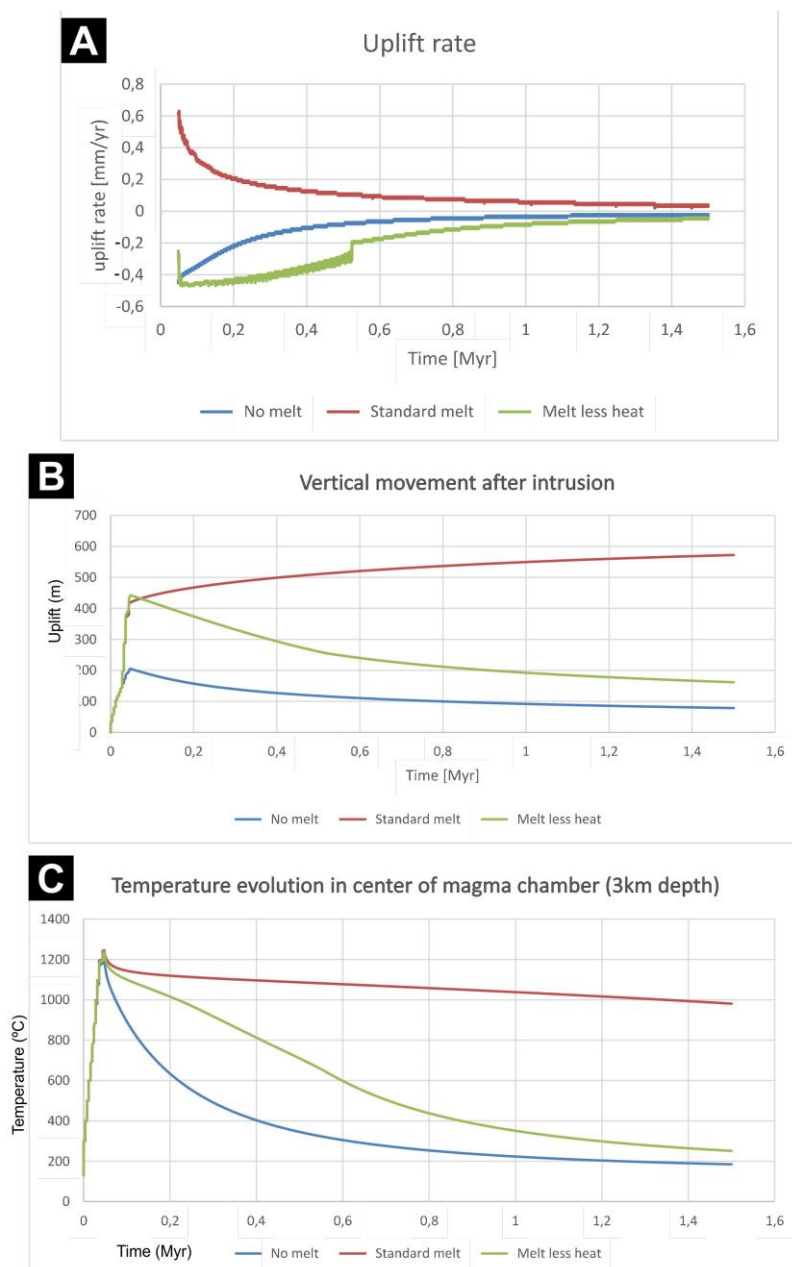
439 Three models were calculated:

440 Model 1 (no melt, blue curve in graphs of Fig. 10): we neglected melt production and let the  
441 intrusion cool down by diffusion. In this case, the reduction of density due to the high  
442 temperature of the intrusion is relatively weak; however, the intrusion cools relatively fast.

443 The resulting maximum subsidence rate at the beginning of thermal relaxation amounts to 0.4  
444 mm/yr.

445 Model 2 (standard melt, red curve in graphs of Fig. 10): we considered the fact that, at 1250 °C,  
446 we are above the liquidus of basaltic rock, and therefore the intrusion should be completely  
447 molten. During cooling, we now must consider the latent heat of basaltic melt, which delays

448 cooling. We used a value of 42 MJ/kg (Lange et al., 1994). On the other hand, the melt has a  
449 much lower density than solid basalt (about 2600-2700 kg/m<sup>3</sup> for melt; e.g. Bajgain et al.,  
450 2015) vs 3000 kg/m<sup>3</sup> for solid rock at room temperature (e.g. Schön, 2004), giving therefore a  
451 stronger topographic effect. For this model, however, due to the large latent heat, cooling is  
452 very much delayed, and it takes about 2 Myr to freeze the whole magma chamber. The effect  
453 on vertical movement is that during the time it takes to freeze the magma chamber, the rocks  
454 around heat up and topography increases. Instead of subsidence, we would observe uplift  
455 during several Myr.



456

457 *Figure 10. Representative graphs of uplift rate (A), vertical movement (B) and temperature*  
458 *evolution at the centre of the intrusion (C) for models 1, 2 and 3.*  
459

460 Model 3 (melt with smaller latent heat, green curve in graphs of Fig. 10): for an intermediate  
461 model, we tested the case of a melt with ten times smaller latent heat than for Model 2. This  
462 model freezes faster and subsides at the fastest rate; however, the difference with respect to  
463 Model 1 is small, and with a maximum of 0.45 mm/yr the subsidence is still much slower  
464 than the currently observed.

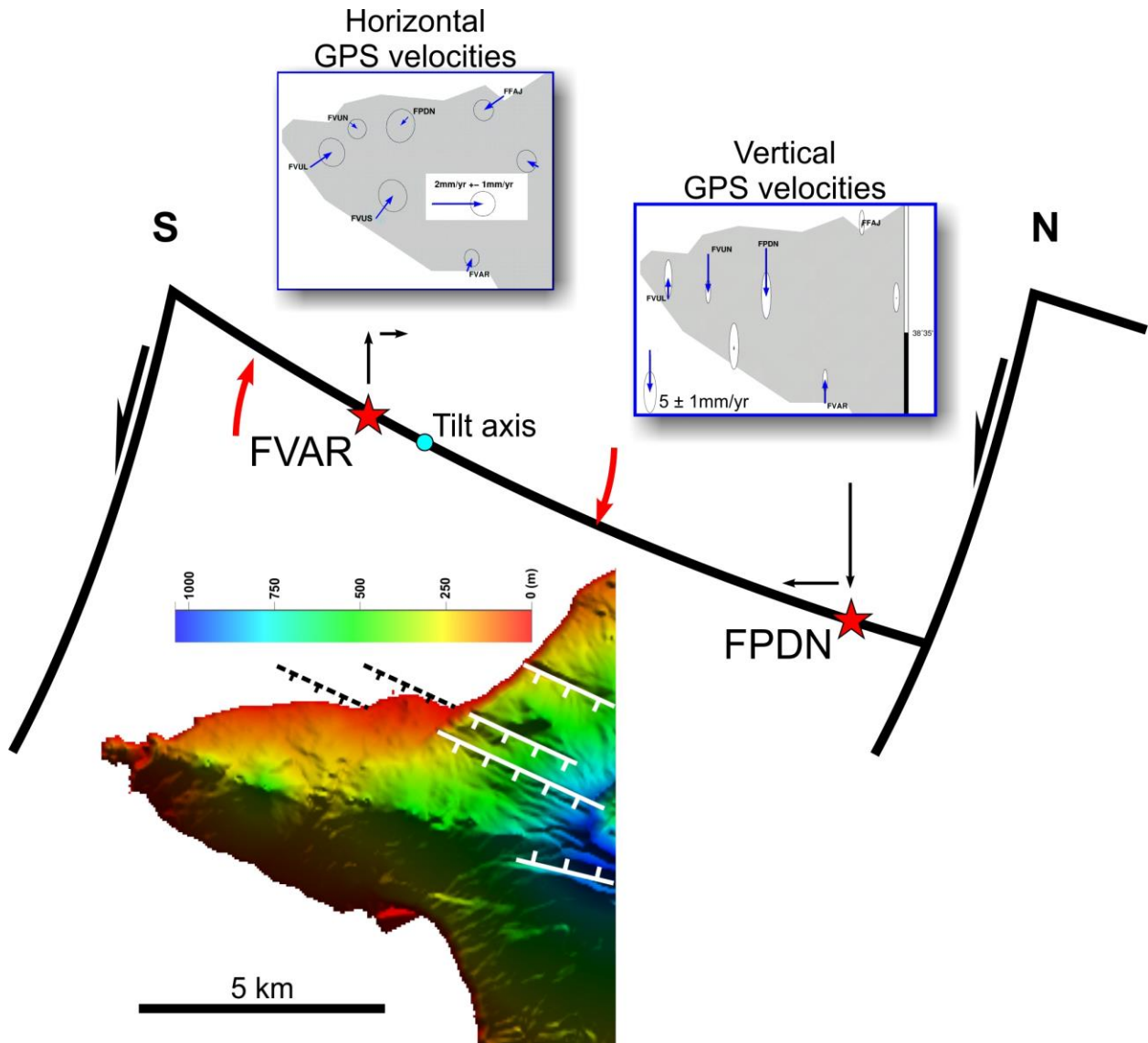
465 Therefore, in a first approximation we can exclude thermal subsidence of a cooling  
466 magma chamber as main reason for the observed differences of vertical movements in the  
467 Capelo area.

468 Given that contraction cannot explain, by itself, the measured GPS vertical velocities, we  
469 have to recourse to the other possibilities. The mechanical hypothesis – upward velocities could  
470 be explained by rising magma, while the downwards velocities could result from flexural effects.  
471 However, this would imply the existence of a layer with an elastic thickness of only ca. 100-300  
472 m, an estimate based on the position of a potential maximum subsidence rate some 5-10 km  
473 away from the centre of the gravity anomaly, corresponding to the centre of the potential magma  
474 chamber (Turcotte and Schubert, 2014), which does not seem realistic, even in a volcanic  
475 environment. The tectonic hypothesis – tectonics by itself fails to explain the localization of  
476 deformation in this area, because no deformation has been observed east of Capelo in graben  
477 faults. The tectonomagmatic hypothesis – to help explain this hypothesis, we drew the sketch  
478 shown in Fig. 11, where we can see that a rotating normal fault can explain the measured GPS  
479 velocities: south of the tilt axis the ground moves upward and to the north, and north of the tilt  
480 axis the ground moves downward and to the south. Why only here at Capelo near the 1957-58  
481 eruption and the gravity anomaly? Probably because the motion of magma in the reservoir (or  
482 withdrawal of magma from the reservoir) and contraction by cooling triggered the motion in the

483 nearby normal faults of the Faial Graben, so showing an intimate relationship between tectonics  
484 and magmatism.

485

486



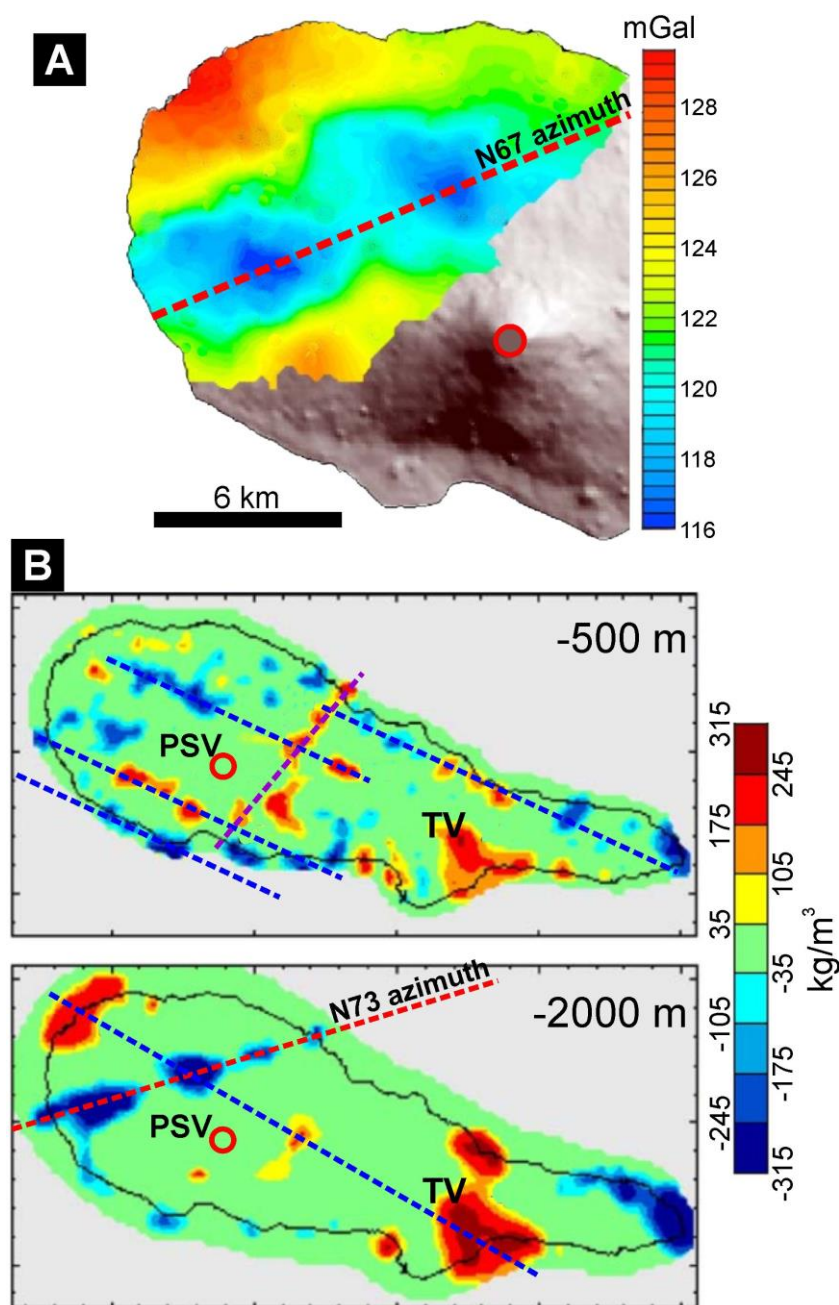
487

488 *Figure 11. Cross-sectional sketch illustrating the tectonic solution for the velocity problem in*  
489 *westernmost Faial.*

490

491 Regarding Pico, the GPS data in Hildenbrand et al. (2012b) were acquired from 2001 to  
492 2006, and showed small horizontal movement, but significant downward movement ( $7 \pm 2$   
493 mm/yr) at Ribeiras (SE Pico Island). The InSAR data collected from 2006 to 2009 and reported

494 in Hildenbrand et al (2012b) were showing also significant subsidence at Ribeiras, but only over  
 495 a limited period. In the present study we report GPS data acquired in the period 2001-2012,  
 496 which shows no movement at the Ribeiras station. This is a question for which we do not have  
 497 an answer, and therefore deserves further investigation.



498  
 499 *Figure 12. Maps of Bouguer anomaly (A) and gravity anomaly (B). From both representations of*  
 500 *the gravity field, it is clear that a lineament of bodies of lower density magma/rock exists at*  
 501 *depth (aligned blue spots below the NW flank of the Pico Volcano), and trends ca. N70 in*  
 502 *azimuth (red dashed lines). Closer to the surface (-500 m in B), two different lineaments can be*  
 503 *interpreted, one striking ca. N115, and the other ca. N50. PSV – Pico Volcano; TV – Topo*

504 *Volcano. Red circle marks the position of Pico's summit. Maps of Bouguer and gravity anomaly*  
505 *cropped and adapted from Figs. 6 and 7, respectively, in Nunes et al. (2006).*  
506

507 In Pico, the gravity data (Fig. 12) shows two contrasting pictures depending on depth: (1)  
508 many small blue (lower density) and red (higher density) spots at -500 m depth, and fewer but  
509 larger spots below -1,000 m; (2) several WNW-ESE lineaments (parallel to the ridge), and fewer  
510 NE-SW lineaments at -500 m depth; (3) fewer but stronger lineaments at -2,000 m, one ENE-  
511 WSW and the other WNW-ESE. The ENE-WSW lineaments are parallel to the transform  
512 direction related to the Terceira Rift and the Nubia-Eurasia plate boundary (Marques et al., 2013;  
513 Marques et al., 2014a), and the WNW-ESE lineaments are parallel to the ridge and underlying  
514 main tectonic trend. The Bouguer anomaly map is very similar to the gravity anomaly map at -  
515 2,000 m depth (cf. Figs. 12A and B), highlighting a conspicuous ENE-WSW lineament of lower  
516 density rock below the northern flank of the Pico Volcano. The lower and higher density  
517 anomalies can be explained with recourse to temperature (higher temperature means lower  
518 density, and vice-versa), or to porosity (e.g. fractured rock along major faults), or to hydration  
519 (different degrees of hydration of the rock at depth), or to composition (which is not consistent  
520 with the undifferentiated nature of the rocks in Pico, although we do not know if they exist at  
521 depth). Noticeably, no positive or negative gravity anomaly is observed below the centre of the  
522 Pico Volcano, in contrast to what we observe below the Topo Volcano (strong positive  
523 anomaly). This can be interpreted in two different ways: (1) there is no high-density vertical  
524 cylindrical feeder below Pico Volcano, in contrast to what was suggested for the Topo Volcano  
525 by Nunes et al. (2006); (2) there is a high-density vertical cylindrical feeder below Pico Volcano,  
526 but its temperature is still warm enough to mask its higher (cold) density; or (3) Pico Volcano is  
527 dominantly composed of massive dense basaltic rocks at depth, which means that a frozen  
528 conduit filled with massive rock (neck) could exist but would not produce a detectable gravity  
529 anomaly.

530

531 *4.2. Marine record*

532           The uppermost strata mainly resemble mass transport deposits similar to S. Miguel  
533 (Sibrant et al., 2015b; Weiß et al., 2015a, b, 2016). In all seismic lines NE, SE and S of Pico the  
534 seismic units P-SJ, T and P have a rather flat unconformity at its upper boundary. Once the Pico-  
535 Faial ridge lies between the profiles, it is not possible to correlate the stratigraphy present in the  
536 seismic lines N and S of Pico. However, the comparable internal reflection configuration, the  
537 similar TWT interval and the location some 10 ms below the seafloor suggest a related genesis.  
538 It should be noted that the diffuse internal reflection pattern of unit P-SJ in the ESE part of the  
539 seismic profile in Fig. 8A is not necessarily related to transport or depositional processes. Based  
540 on gravity core GC36, marked in Fig. 8A, Schmidt et al. (2020) inferred that the cored area is  
541 hydrothermally active, and therefore attributed the weak internal reflection amplitudes and the  
542 presence of phase reversed reflections to increased fluid content. However, the chaotic or  
543 contorted internal stratification rule out that these are hemipelagic deposits. Hence, there are  
544 basically two different endmembers to interpret these units, which are debris avalanche deposits  
545 (DAD) from flank collapses of an established volcanic edifice, or deposits resulting from  
546 pyroclastic flows. Based on observations from the vicinity of Montserrat Island, Karstens et al.  
547 (2013) inferred that the coarse and denser material of pyroclastic flows is deposited close to the  
548 coast. It is only the fine-grained ash fraction that forms a turbidity current and can spread out  
549 over long distances. The resulting turbidite deposits are characterized by a flat top, which is  
550 consistent with the units P-SJ, T and P. However, contrary to the units observed here, the internal  
551 bedding of upward fining turbidites is expected to be rather parallel. We therefore consider this  
552 interpretation as unlikely. Furthermore, neither Pico nor S. Jorge islands show onshore evidence  
553 for violent pyroclastic eruptions (only local strombolian cone deposits). Faial has experienced  
554 large differentiated explosions, but the related pyroclastic deposits (pumice fallout) do not crop

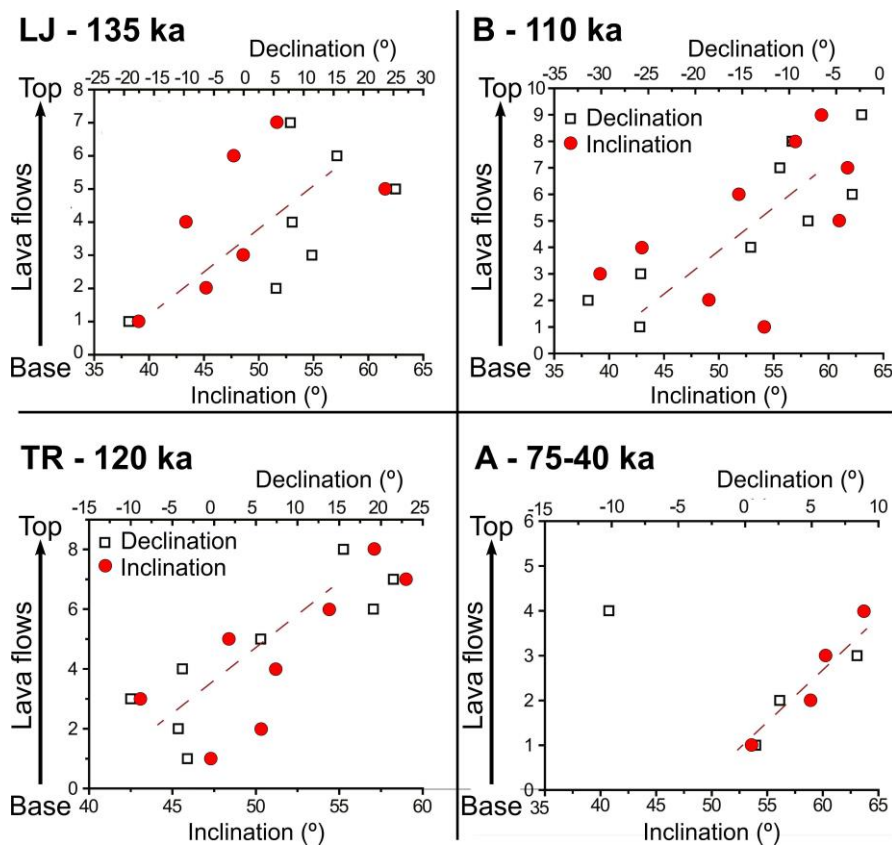
555 in S. Jorge and Pico, so the upper layer of submarine products here imaged offshore the eastern  
556 half of Pico are unlikely to represent large pyroclastic flows. As discussed by Karstens et al.  
557 (2013), sub-aerial debris avalanches result in the submarine emplacement of block-rich deposits  
558 that form as the failing host rock is broken down through a process of fracturing and internal  
559 block-to-block collision (Pollet and Schneider, 2004). These blocks, combined with internal  
560 deformation processes, may create a hummocky topography and a very chaotic internal structure  
561 (e.g. Krastel et al., 2001; Hildenbrand et al., 2006; 2018). Such a hummocky upper boundary is  
562 not observed around Pico (Fig. 8). However, Karstens et al. (2013) presented high-resolution  
563 seismic reflection data from DADs off Montserrat, which have similar thicknesses as units P-SJ,  
564 T and P, and which also reveal internal contorted reflections and thrusts. The flat upper  
565 unconformity of the DADs around Pico can be explained by the fact that the sliding avalanche  
566 body absorbs more water during its transport and thus becomes more fluid. The flat to  
567 hummocky lower unconformity implies that units P-SJ, T and P overlie older DAD, which could  
568 be related to Topo's destruction. The origin of unit P-SJ is not unambiguous. The debris  
569 avalanche may have come from either Pico or S. Jorge. The bathymetric data show amphitheatre  
570 like, arcuate escarpments on and offshore N and NE Pico, and on the southern shelf edge of S.  
571 Jorge. However, the bathymetry shown in Fig. 4 of Costa et al. (2014) clearly indicates a source  
572 of the DAD on Pico's northern flank. The interpretation of unit T right in front of the lower slope  
573 is less ambiguous, because internal folds and thrusts are clear indicators for DAD. The polarity  
574 change above the thrusts may result from compaction and resulting dewatering. The location SE  
575 of ancient Topo and the volume suggest that unit T represents the deposits of a sector collapse of  
576 Topo (see Costa et al., 2015). The location SE of Pico Volcano and the young character of the  
577 deposit suggest that unit P (Fig. 8E, F) represents the DAD of a flank collapse of Pico Volcano,  
578 as hinted by the asymmetry of this volcano (missing flank as inferred in Fig. 3B, C).

579 The limited data coverage does not allow estimating the entire volume of the up to 100 m

580 thick DAD in the central part of Fig. 8C. As a very coarse estimate, we assume that the main  
 581 deposits cover a circular area with a diameter of 7 km. If we assume a thickness of 75-100 m  
 582 (100 ms TWT), the deposits make up 3-4 km<sup>3</sup>. There are no samples that would allow for a  
 583 precise Dense Rock Equivalent (DRE). However, if we assume a factor of 0.7 (e.g. Johnston et  
 584 al., 2015), we end up with an estimated DRE of 2-3 km<sup>3</sup>. Since we did not consider deposits  
 585 outside the 7 km circle, this estimate is rather conservative.

586 From both the bathymetry and seismic profiles, it is clear that VCs are abundant S and SE  
 587 of Topo. Dykes' trend in southern Topo (cf. Fig. 3B in Costa et al., 2014) as well as the  
 588 previously described change in the strike direction of Pico ridge align along a WSW-ENE trend  
 589 that is parallel to an inferred transform fault further NW (Marques et al., 2014a). We therefore  
 590 suggest that another transform fault runs along the eastern ends of Pico and S. Jorge towards the  
 591 Terceira Island in the Terceira Rift (Fig. 7A).

592



593

594 *Figure 13. Graphs with declination and inclination of characteristic remanent magnetization*

595 *(ChRM) along individual lava flow sequences (LJ, TR, B and A, from older to younger), with the*  
596 *main trends represented by red dashed lines. Note that graphs are very similar for sequences LJ*  
597 *and TR, these in turn somewhat similar to sequence B, and these three different from sequence A*  
598 *(youngest). Also note that, in each sequence, both declination and inclination vary by many*  
599 *degrees, except for sequence A (only 10°). Graphs adapted (no changes made to the data) from*  
600 *Fig. 7 in Silva et al. (2018).*  
601

#### 602 *4.3. Palaeomagnetic data*

603 Paleomagnetic data in Faial is consistent with the tectonic activity in the Faial Graben,  
604 i.e. the measured rotations are consistent with uplift on the graben shoulders and rotational  
605 normal faults (cf. Fig. 6 in Silva et al., 2018).

606 Palaeomagnetic data in Pico is more complex and thus susceptible of different  
607 interpretations. The graphs in Fig. 13 display the declination and inclination of characteristic  
608 remanent magnetization (ChRM) along individual lava flow sequences. These graphs show that  
609 trends and magnitudes are very similar for sequences LJ (ca. 135 ka) and TR (ca. 120 ka), which  
610 in turn are somewhat similar to sequence B (ca. 110 ka), and all these three are different from  
611 sequence A (75 to 40 ka). Noticeably, in each sequence both declination and inclination vary by  
612 many degrees, except for sequence A (only 10°). The graphs in Fig. 13 can be interpreted in two  
613 contrasting ways: (1) as cumulative (the oldest represents the accumulation of younger events),  
614 or (2) as reflecting non-cumulative individual events. If the rotations were cumulative, then one  
615 would go to the field and measure very steep flows (ca.  $25^{\circ}+15^{\circ}+25^{\circ}+10^{\circ} = 75^{\circ}$ ), which is  
616 certainly not the case. The problem is also that the 10° rotation in sequence A, the youngest  
617 sequence, cannot justify the rotations measured within each of the older lava flow sequences. At  
618 most, it can be responsible for a 10° rotation, which is small compared to the rotations measured  
619 in the older sequences. The inferred rotation in sequence B cannot be responsible for the ChRMs  
620 measured in the older LJ and TR sequences too, because these also rotate individually. From this  
621 we can infer cyclicity of rotations in the lava flow sequences over time, and propose a new  
622 interpretation: the measured inclinations are the product of inflation and deflation cycles in a

623 magma reservoir, which reset the tilting between cycles in overlying lava flows, being the  
624 inferred rotation the result of inflation or deflation depending on the position of the magma  
625 chamber relative to the overlying flows. In the present case, the magma chamber would have to  
626 lie to the northeast of the analysed lava flows, because the vertical rotation is to the south, and  
627 the horizontal rotation is clockwise. Marques et al. (2013, 2014b) and Costa et al. (2014, 2015)  
628 have shown that the Pico-Faial ridge lies on the shoulder of a graben, but this cannot explain the  
629 measured tilting because it would have to be cumulative.

630         The inferred inflation/deflation cycles could be, at least in part, responsible for the  
631 triggering of the detected flank collapses, as such cycles can fracture the rocks and make lava  
632 flows and pyroclasts steeper during inflation. The fact that the paleomagnetic data refer to  
633 samples collected on both blocks of a main fault along which a large-scale flank collapse  
634 occurred is not considered a coincidence here. On the contrary, we suggest a cause-effect  
635 relationship, i.e. inflation/deflation (cause) related to large-scale landslide (effect). Therefore,  
636 inflation/deflation cycles can also contribute significantly to the shaping of the volcanic island.

637

#### 638 *4.4. Petrographic and geochemical data*

639         Pico and Faial both comprise central and fissure volcanism, whose petrographic and  
640 geochemical characteristics have been described previously and are summarised here (França et  
641 al. 2006; Beier et al., 2012; Zanon et al. 2013, 2020; Zanon and Frezzotti 2013; Métrich et al.  
642 2014).

643         The lavas emitted by both volcanic systems belong to the alkaline series (Beier et al., 2012)  
644 with  $\text{Na}_2\text{O} > \text{K}_2\text{O}$ . The lavas erupted in the fissure systems of the two islands are basalt to  
645 trachybasalt. Mugearites on Pico Volcano are volumetrically very reduced, because they are  
646 exclusive of the first phases of the small 1718 eruption. In contrast, large volumes of trachyte  
647 pumice were erupted in Faial and blanketed most of the island during late-stage magmatic events

648 from Caldeira Volcano in the last 12 ka. These differences could be related to the different ages of  
649 volcanism found in Faial and Pico, with Faial being older and more differentiated.

650 In Faial, there are no significant textural differences among the mafic lavas erupted by  
651 fissure systems and Caldeira Volcano; both are poorly porphyritic (phenocrysts content  $\leq 25\%$ )  
652 with a mineral assemblage constituted by mafic phenocrysts ( $\varnothing = 1.5\text{--}6.0$  mm) and plagioclase.  
653 The composition and abundance of the phenocrysts in the mafic lavas is, in general, similar in all  
654 volcanic complexes, with Fe-Mg olivine (Mg#=77-82), clinopyroxene augite (Mg#=72-86),  
655 plagioclase (from andesine to bytownite) and Fe-Ti oxides (titanomagnetite and ilmenite). In  
656 contrast, on Pico Volcano the lavas poured from lateral vents are highly porphyritic (up to 70%  
657 phenocrysts) with a mineral assemblage comprising olivine antecrysts (up to Fo86%) and  
658 megacrysts of clinopyroxene (up to 25 mm in length) that show the same composition of the  
659 phenocrysts. Plagioclase is commonly absent, and oxides are represented by titanomagnetite. The  
660 recent lavas of the cone at the top of the volcano are porphyritic (up to 35–40 vol% of phenocrysts),  
661 with mineral assemblage represented by euhedral plagioclase (up to 1.8 cm), a few clinopyroxenes  
662 ( $\varnothing \leq 2.2$  mm) and rare olivine microphenocrysts ( $\varnothing = 0.25\text{--}0.45$  mm).

663 Beier et al. (2012) inferred that the Azores lavas are consistent with peridotite melting at  
664 normal oxygen fugacity, and assumed that the measured differences in SiO<sub>2</sub>, total FeO and, in  
665 particular, TiO<sub>2</sub> in the Faial and Pico lavas solely reflect changes in melting pressures and  
666 temperatures. Beier et al. (2012) concluded for a broad range of melting pressures in central  
667 Azores, with shallower melting underneath Faial than underneath Pico. Prytulak and Elliott (2009)  
668 concluded differently, i.e. for a garnet peridotite source beneath Pico from <sup>238</sup>U-<sup>230</sup>Th and <sup>235</sup>U-  
669 <sup>231</sup>Pa disequilibria. Additionally, the differences in the silica saturation degree and the ratios  
670 between very incompatible elements in the most primitive samples suggest two lithologically  
671 different mantle sources. This can be inferred from the different helium isotopic signatures too: in  
672 Faial, the ratio R/Ra is in the range 7.2-8.7 (Moreira et al., 1999), which straddle the MORB lavas

673 emitted at the Mid-Atlantic Ridge ( $\sim 8 \pm 1$  R/Ra; e.g. Parman, 2007). Differently, lavas from Pico  
674 show R/Ra in the range 10.5-11.2 Ra (Moreira et al., 1999; Métrich et al., 2014), which is more  
675 like the higher ratio typical of primitive sources.

676 The critical differences, observed in Faial and Pico between the closely spaced fissural and  
677 central volcanisms could be the result of different plumbing systems: WNW-ESE faults  
678 responsible for the fissural volcanism with similar orientation, and intersection between the  
679 WNW-ESE and ENE-WSW fault systems responsible for the central volcanism. The age of the  
680 volcanism is also critical, but cannot justify differences when the lavas are of similar age.  
681 Additionally, there are also differences between the lavas in the two islands despite belonging to  
682 the same ridge and being close to each other. Beier et al. (2012) suggested that small-scale source  
683 heterogeneity is not related to the major element systematics, but reflects changes in melting  
684 pressures and temperatures, which could be related to distance from the Mid-Atlantic Rift and,  
685 therefore, to lithospheric thickness.

686 To summarize, the petrological/geochemical data indicate why the volcanic morphology is  
687 markedly different in the two islands, and the influence the different magmas have on the  
688 morphology of the central volcanoes: basaltic, very tall cone (although younger; < ca. 60 ka) and  
689 small crater in Pico, and basalt to trachyte, shorter cone (half height although twice older; < ca.  
690 130 ka) with quite large and deep caldera in Faial.

691

692 *4.5. Evolution of the Pico-Faial ridge*

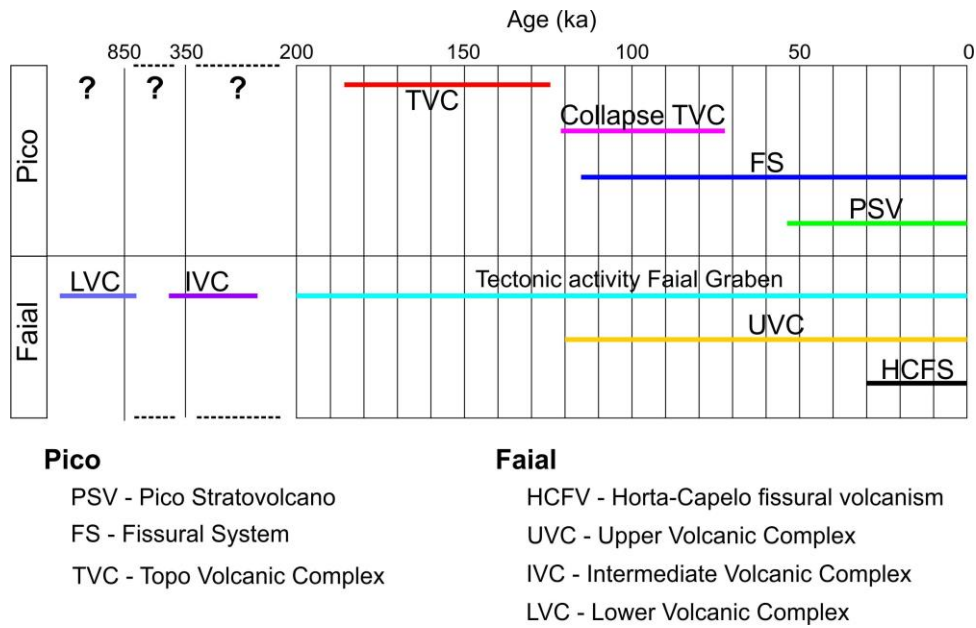
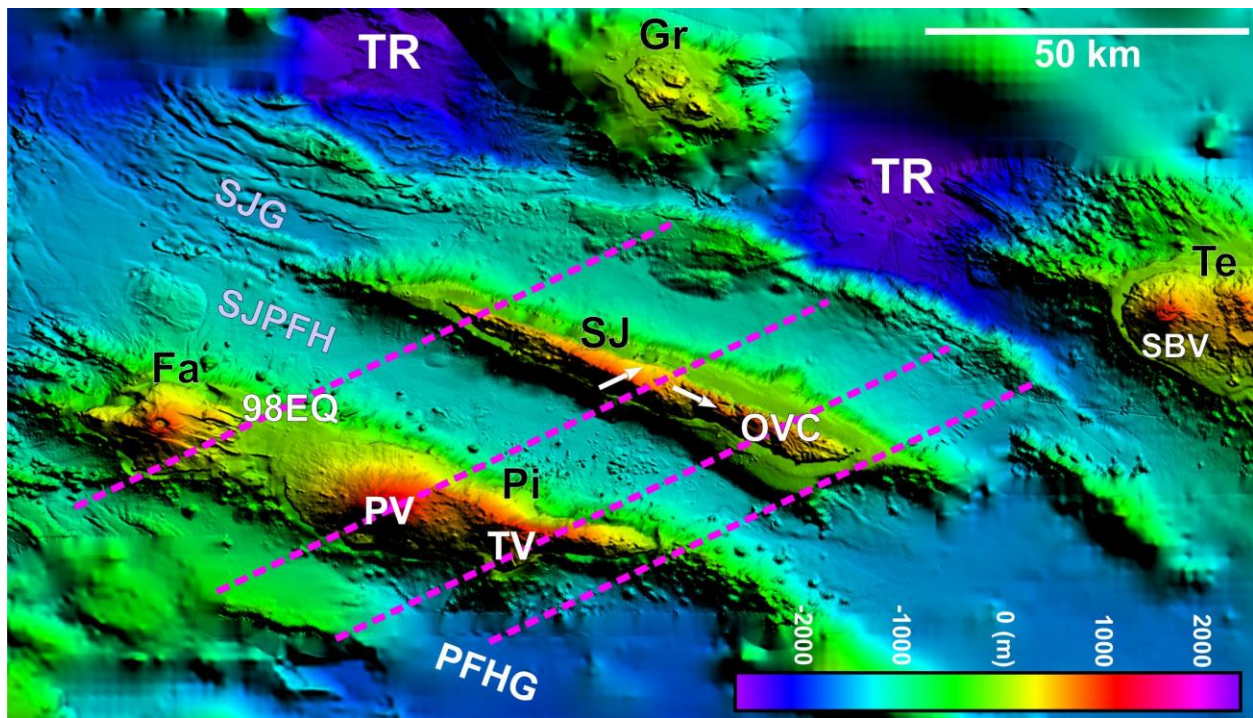


Figure 14. Timeline of the compared evolutions of Pico and Faial in the last 1 Ma.

The oldest volcanism in Faial and Pico seems to have been made up of isolated central volcanoes or shield volcanoes, therefore originally not comprising a true volcanic ridge at the surface. Maybe it was a submarine ridge on top of which the central volcanoes grew out of the ocean. In Faial, the oldest volcanism was constrained at around 850 ka (Hildenbrand et al., 2012a). As described by Romer et al. (2018), the seafloor topography west of Faial reveals large submarine volcanic rift zones, including that of the 1957–1958 Capelinhos eruption. These authors concluded that the formation of WNW-ESE oriented narrow submarine structural and magmatic features since ca. 1 Ma likely resulted from extensional stresses, showing that lithospheric extension is an important process during the evolution of the subaerial and submarine volcanic structures, which is consistent with the current GPS data and conclusions in Marques et al. (2013).



706  
 707 *Figure 15. Shaded relief of the islands in the Azores Central Group. Dashed magenta lines*  
 708 *represent our interpretation of the position of ENE-WSW transform faults related to the*  
 709 *kinematics in the diffuse boundary between the Eurasia and Nubia plates. Fa – Faial; Pi – Pico;*  
 710 *SJ – S. Jorge; Gr – Graciosa; Te – Terceira. SJG – S. Jorge Graben; SJPFH – S. Jorge/Pico-*  
 711 *Faial Horst; PFHG – Pico-Faial Half-graben. 98EQ – location of the 1998 Faial earthquake;*  
 712 *PV – Pico Volcano; TV – Topo Volcano; OVC – Old Volcanic Complex in S. Jorge Island; SBV*  
 713 *– Santa Bárbara Volcano in Terceira Island. White arrows on S. Jorge Island represent the main*  
 714 *GPS velocities. Background image from EMODnet portal ([https://www.emodnet-](https://www.emodnet-bathymetry.eu/)*  
 715 *bathymetry.eu/).*  
 716

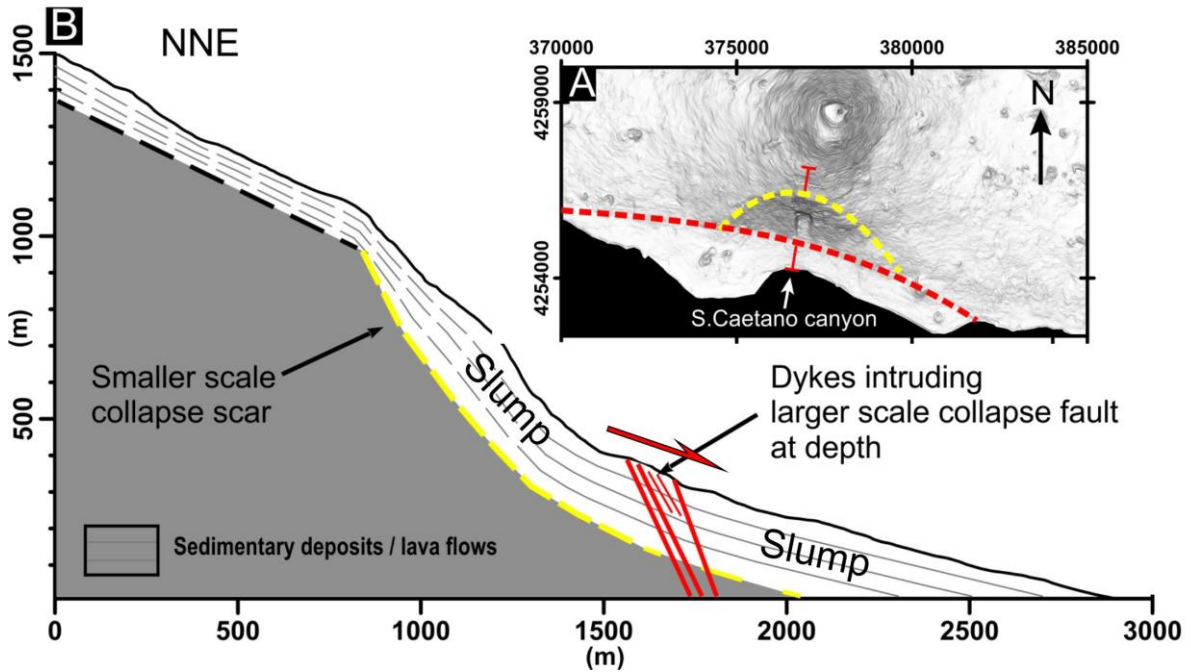
717 In contrast to Faial, the oldest sub-aerial volcanism in Pico is much younger than 850 ka.  
 718 The sub-aerial growth of the Topo Volcano in Pico was constrained between ca.  $186 \pm 5$  and  $125$   
 719  $\pm 4$  or  $115 \pm 4$  ka (Costa et al., 2014, 2015). Given the present morphology of the Topo Volcano  
 720 and the attitude of the lava flows, the summit of the Topo Volcano should have been originally  
 721 located atop the positive gravity anomaly detected in this area (Nunes et al., 2006).

722 Based on the position of the four main central volcanoes (two in Faial and two in Pico),  
 723 the main lithospheric trends, the GPS velocities in S. Jorge (Mendes et al., 2013), the position of  
 724 the Old Volcanic Complex in S. Jorge (Marques et al., 2018), the location of the Faial 1998  
 725 earthquake (Marques et al., 2014b), and recently recognized faults (e.g. Sibrant et al., 2015b,

726 2016), we infer that the central volcanoes developed at the intersection of major lithospheric  
727 faults, mainly the WNW-ESE and ENE-WSW fault systems (Fig. 15) (see also Zanon et al.,  
728 2020). The ENE-WSW faults are parallel to the velocity vectors representing the motion  
729 between Eurasia and Nubia (also ENE-WSW), and could thus correspond to transform faults  
730 related to the Terceira Rift and diffuse Eurasia/Nubia plate boundary. As shown in Fig. 15, we  
731 suggest the existence of four transform faults cutting across the Pico-Faial Ridge, which can  
732 justify the position of the central volcanoes, major earthquakes, and faults inferred from the  
733 seismic lines.

734         The several scars that affect the central/eastern part of the Pico Island, in both south and  
735 north flanks, point to repeated episodes of flank collapse. So far, the evidence came from GPS and  
736 InSAR data (Hildenbrand et al., 2012b) and digital elevation models of both on and offshore  
737 topography (Costa et al., 2014, 2015). Now we add evidence from seismic profiles acquired  
738 offshore the ridge. The remnants of the Topo Volcano are partly exposed on Pico's SE flank, and  
739 have been dated between ca. 186 and 125 ka by Costa et al. (2015), who concluded that Topo was  
740 significantly destroyed by N- and S-directed large-scale flank collapses between ca. 125 and 70  
741 ka. There is no direct evidence that there was a volcanic ridge contemporaneous with Topo, but  
742 we cannot exclude the possibility that a submarine ridge existed prior to the Topo Volcano, on  
743 which this volcano grew.

744         The ages obtained by Costa et al. (2014, 2015) indicate that the Pico Volcano developed  
745 during the last 50 ka. This points to a concentration of the volcanism on the western side of the  
746 island, with the fast construction of an impressive and still active volcano within only a few tens  
747 of thousands of years. Contemporaneous volcanic activity occurred along the main Fissural  
748 System and in the slump area in SE Pico.



749  
 750 *Figure 16. Interpretation of the topographic profile along the S. Caetano canyon and*  
 751 *observations presented in Fig. 4. (A) Shaded relief of the Pico Volcano's southern flank (vertical*  
 752 *lighting), with indication of the trace of the cross section presented in (B), drawn along the S.*  
 753 *Caetano canyon. (B) Topographic profile along the S. Caetano canyon (no vertical*  
 754 *exaggeration). The dip of the observed dykes and lava flows/sedimentary deposits are*  
 755 *represented. The yellow dashed line represents the base of the inferred slump, and the red lines*  
 756 *represent the observed dykes intruding the slump and an underlying fault of a larger flank*  
 757 *collapse. Red half-arrow indicates the sense of shear inferred from the en échelon arrangement*  
 758 *of the dykes.*

760 Regarding the WNW-ESE scarp on the southern flank of Pico Volcano, previously  
 761 published works only mention that this scarp was covered by volcanic deposits from the volcano,  
 762 and that there are significant recent colluvium deposits along the base of the scarp (Chovelon,  
 763 1982; Madeira, 1998; Nunes, 1999). Our field observations add to the published work regarding  
 764 this scarp. In the S. Caetano canyon, as we did not observe a large-scale unconformity, we  
 765 propose that the sequences observed on the scarp are concealing a larger-scale failure surface  
 766 (Figs. 3B, C and 16). These sequences of volcano-sedimentary material and lava flows are cut by  
 767 numerous dykes disposed *en échelon*, which strike parallel to the main scarp and dip downstream  
 768 (Figs. 4 and 16). The local *en échelon* arrangement of the dykes suggests that the intruded

769 volcano-sedimentary sequence was undergoing shear deformation (creep with top to the south)  
770 during intrusion (Fig. 16), consistent with the motion of a slump. Given that part of the deposit in  
771 the S. Caetano canyon is made up of sediments, then we infer that there was an earlier collapse  
772 that later was filled with sediments and flows intruded by dykes. These dykes seem to have  
773 intruded the fault of a larger flank collapse represented by the red dashed line in Fig. 16A.  
774 Furthermore, the possibility of future structurally controlled dyke intrusion along this scarp, as  
775 the Pico Volcano has been historically active, suggests that this sector is prone to landslide  
776 occurrence. The local steepness of the topography can be an effect of an earlier landslide (see  
777 seismic profile in Fig. 8E), and the inferred slumping indicates that this scarp is prone to further  
778 landsliding.

779

## 780 **5. Conclusions**

781 The compared evolution of Pico and Faial islands shows that Faial comprises the oldest  
782 sub-aerial volcanism dated at ca. 850 ka (Hildenbrand et al., 2012a), probably lying on a  
783 submarine ridge of unknown age. This early subaerial volcanism was followed by ca. 500 ka of  
784 destruction of the original central volcano, but we have not found yet evidence for the type of  
785 erosion: large-scale collapse(s) or long-term marine erosion? Around 360 ka, a new edifice was  
786 growing in NE Faial, and still with no counterpart in Pico. This younger volcano was also  
787 partially destroyed before being unconformably overlain by younger volcanism associated with  
788 the Caldeira Volcano, which rapidly grew during a main phase of activity between ca. 130 and  
789 115 ka. The equivalent of the older construction/destruction activity in Faial (> 200 ka) has not  
790 been found in Pico, despite belonging to the same volcanic ridge. Based on published work and  
791 new data and interpretations, here we propose the following evolution of the Pico-Faial ridge for  
792 the last 200 ka: (1) In Faial, a WNW-ESE island-scale graben, the Faial Graben, started  
793 developing sometime prior to ca. 130 ka, the age of lavas already flowing between fault scarps

794 making up the graben. Meanwhile, the sub-aerial Topo Volcano was growing in Pico (ca. 186-  
795 125 ka). (2) While Topo was reaching its final stages of growth in Pico and being dismantled (ca.  
796 125-115 ka), a central volcano (the Caldeira Volcano) was rapidly growing in Faial (ca. 130-115  
797 ka, Hildenbrand et al., 2012a), partially filling the central depression of the Faial Graben. (3)  
798 Between ca. 115 and 70 ka, there was considerable sub-aerial growth and destabilization of the  
799 Fissural System in Pico. Major catastrophic flank collapses occurred prior to 70 ka in both north  
800 and south flanks of Pico Island. The DADs have thicknesses of up to 75-100 m. A DAD,  
801 presumably resulting from collapsing Topo to the south has a DRE of at least 2-3 km<sup>3</sup>. In  
802 contrast to the large-scale destruction in Pico, the Caldeira Volcano in Faial is mostly preserved  
803 except for the mild disruption caused by the tectonic activity in the Faial Graben. (4) Since ca. 50  
804 ka, the Pico Volcano has been growing on the westernmost sector of the island. In contrast to the  
805 well preserved, though older, Caldeira Volcano, the S flank of the Pico Volcano seems to have  
806 suffered a partial flank collapse as hinted by its asymmetry and inferred from marine seismic  
807 profiles. At ca. 50 ka, the Faial Graben was fully developed, with tall scarps producing  
808 conglomerates later covered by lava flows flowing from the Caldeira Volcano down the Faial  
809 Graben towards the sea in the east. (5) In the last 10 kyr, extended volcanic activity has occurred  
810 in the Pico Volcano, the Fissural System, and as parasitic activity on Topo's SW flank. A slump  
811 is currently active in SE Pico (Hildenbrand et al., 2012b). In Faial and since ca. 10ka, a WNW-  
812 ESE sub-aerial Fissural Complex grew towards the W, and episodes of explosive activity  
813 occurred in the Caldeira Volcano and covered most of Faial with a pumice deposit (Madeira and  
814 Brum da Silveira. 2003). Such voluminous differentiated, trachytic pumice deposits have not  
815 been found in Pico. The volcanic activity in Faial culminated with the recent Capelinhos eruption  
816 in 1957-1958, which stretched the island to the west. Tectonic activity (normal faulting)  
817 triggered by the feeder of the Capelinhos eruption may be responsible for the measured  
818 anomalous GPS velocities in westernmost Faial.

819

## 820 **Acknowledgments**

821           This is a contribution to Project MEGAHazards2 (PTDC/GEO-GEO/0946/2014), funded  
822 by FCT, Portugal. ACGC's Postdoctoral scholarship was funded by the Alexander von  
823 Humboldt Foundation. Special thanks to Judite Costa, José Costa, José Dias and Nilton Nunes  
824 for support during fieldwork.

825

## 826 **Supplementary material**

### 827 *DEM analysis*

828           The interpretation of shaded relief and slope maps constructed from the synthetic grid  
829 allowed us to distinguish and characterize different morpho-structural features. A 10 m  
830 resolution sub-aerial DEM was complemented with bathymetric data acquired offshore Pico (see  
831 Costa et al., 2014, 2015, and Hübscher et al., 2016 for details), aimed at identifying landslide  
832 scars and potential debris deposits generated by mass wasting episodes.

833

### 834 *GPS data and processing*

835           The Faial-Pico GNSS geodetic-geodynamic network was established in 2001 in the aim  
836 of STAMINA and SARAZORES research projects (Navarro et al., 2003; Catalão et al., 2006). It  
837 consists of 20 stations with metallic benchmarks installed on outcrops of solid rock distributed  
838 mostly around the perimeter of both islands, with an average spacing of ca. 5 km (Fig. 001). The  
839 data used in this study were acquired during six surveys in the period 2001 to 2012. Each site  
840 was surveyed for 12 to 24 hours per day, over an average of 3 consecutive days. All the surveys  
841 were performed using dual-frequency GPS receivers, collecting data every 30 sec and elevation  
842 mask of 15°. During each survey, at least six stations were observed simultaneously, and one  
843 station was measuring continuously (FAIM). For this 12-year long time series, each station was

844 visited at least four times and observed for at least eight 24-hours sessions.

845           GPS data were analysed using the GAMIT/GLOBK software version 10.6 (Herring et al.,  
846 2010) in a two-step approach as described in Dong et al. (1998). In the first stage of processing,  
847 the station coordinates, the zenith delay of the atmosphere at each station, and orbital and Earth  
848 orientation parameters (EOPs) were estimated using doubly differenced GPS phase observations.  
849 At this stage in the processing, we included GPS data from IGS (International GNSS Services)  
850 continuous operating stations, in order to serve as ties with the ITRF2014 (Altamimi et al.,  
851 2016). We have selected the IGS stations closest to the Azores and located on the Eurasia, North  
852 America, and Nubia plates, and worldwide IGS stations working continuously since 2001. The  
853 ITRF14 used global station coordinates and EOP provided by GNSS and other space geodetic  
854 techniques data time series to update solutions from past years (i.e., 2008). A set of about 40  
855 International GNSS Service (IGS) stations spread across the globe were grouped, in order to  
856 assure precise coordinate estimates and lower correlation for the atmospheric parameters. IGS  
857 precise final orbits were also used. The GAMIT solution was computed using loose constraints  
858 on the a priori station coordinate (0.5 m), a priori hydrostatic and wet models from Saastamoinen  
859 (1972, 1973), and Global Mapping Functions (Böhm et al., 2006). In a second step, daily  
860 GAMIT solutions were used as quasi-observations in GLOBK to obtain the position time series  
861 for all sites. In this solution, the regional daily solutions were combined with the global daily  
862 solution from more than 100 IGS stations computed by SOPAC, the h-files (GAMIT interchange  
863 format). The position time series were analysed to detect and remove outliers, and detect  
864 possible vertical offsets caused by erroneous antenna height. After editing, the site coordinates  
865 and velocities were estimated with respect to ITRF2014 reference frame from a priori values of  
866 coordinates and velocities of IGS permanent sites. The one-sigma uncertainties for the GPS  
867 velocities of our sites were derived by scaling the formal errors by the square root of chi-square  
868 per degree of freedom of the final adjustment. The chi-square per degree of freedom for this

869 solution was 1.05, indicating a reasonable constraint and a robust estimation of parameters.

870 About 50% of the sites have horizontal velocity uncertainties lower than 1 mm/yr.

871

### 872 *Marine geophysics*

873 Seismic reflection and multibeam data used in this study have been collected during  
874 research expedition M113 of RV METEOR in 2015 (Hübscher et al., 2016). The seismic signals  
875 were generated by means of an array of three GI (Generator-Injector)-sources and one Mini-GI-  
876 source towed at a depth of ca. 2.5 m behind the ship's stern. The volume of one GI-source was  
877 45 in<sup>3</sup> for the generator with a 105 in<sup>3</sup> injector volume. The operation mode of this source was  
878 "true GI mode". Two GI-sources had a generator and injector volume of 105 in<sup>3</sup> each, and were  
879 operated in the "harmonic mode". The active sections of the digital streamer had a length of 600  
880 m and comprised 144 channels. Processing included velocity determination, nmo (Normal  
881 MoveOut)-correction, stacking, time-migration and white noise removal. For more details of the  
882 marine seismic method, see Hübscher and Gohl, 2014. Multi-beam data recorded with the Hull  
883 mounted EM122 SIMRAD system and were gridded after editing with 50 m cell size.

884 Additional profiles were built in 2017, during expedition M141, using a 6000-Joule sparker  
885 that created the seismic signal that was recorded by means of a 48-channel analogue cable.  
886 Processing included velocity determination, nmo-correction, stacking, time-migration and white  
887 noise removal.

888

### 889 *Paleomagnetic data*

890 46 lava flows were sampled using a portable gasoline-powered drill. Samples were  
891 collected in lava piles comprising many flows, and 10 to 14 cores were commonly sampled in  
892 each lava flow. We measured the attitude of lava flows cautiously because of the effect of the  
893 irregular topography at the time of flow emplacement. In Faial, sampling focused mainly on lava  
894 flow piles outcropping on main fault scarps at the eastern coast of the island. In Pico, samples

895 were collected along four lava piles of the Topo-Lajes Volcanic Complex, on both sides of the  
896 main fault of the Ribeirinhas slump. Lava piles from sections P-TR and P-LJ are located west of  
897 the main fault and belong to the oldest volcanic unit (Topo Volcano). The other two sections (A  
898 and B) are younger and located to the east of the main slump fault. For detailed information on  
899 sampling strategy and methods see Silva et al. (2018).

900

## 901 **References**

- 902 Altamimi, Z., Rebischung, P., Métivier, L., Collilieux, X., 2016. ITRF2014: A new release of the  
903 International Terrestrial Reference Frame modelling nonlinear station motions. *J. Geophys.*  
904 *Res. Solid Earth* 121, 6109–6131.
- 905 Bajgain, S., Ghosh, D.B., Karki, B.B., 2015. Structure and density of basaltic melts at mantle  
906 conditions from first-principles simulations. *Nature Communications* 6 (8578), doi:  
907 10.1038/ncomms9578.
- 908 Béguelin, P., Bizimis, M., Beier, C., Turner, S., 2017. Rift–plume interaction reveals multiple  
909 generations of recycled oceanic crust in Azores lavas. *Geochim. Cosmochim. Acta* 218, 132-  
910 152.
- 911 Beier, C., Turner, S., Plank, T., White, W., 2010. A preliminary assessment of the symmetry of  
912 source composition and melting dynamics across the Azores plume. *Geochem. Geophys.*  
913 *Geosyst.* 11, Q02004, doi:10.1029/2009GC002833.
- 914 Beier, C., Haase, K.M., Turner, S.P., 2012. Conditions of melting beneath the Azores. *Lithos*  
915 144-145, 1-11.
- 916 Böhm, J., Werl, B., Schuh, H., 2006. Troposphere mapping functions for GPS and very long  
917 baseline interferometry from European Centre Medium-Range Weather Forecasts operational  
918 analysis data. *J. Geophys. Res.* 111, B02406, <http://dx.doi.org/10.1029/2005JB003629>.
- 919 Bonatti, E., 1990. Not so hot ‘hot spots’ in the oceanic mantle. *Science* 250, 107-111.

920 Borges, J. F., Bezzeghoud, M., Buforn, E., Pro, C., Fitas, A., 2007. The 1980, 1997 and 1998  
921 Azores earthquakes and some seismo-tectonic implications. *Tectonophysics* 435, 37–54.  
922 <http://dx.doi.org/10.1016/j.tecto.2007.01.008>.

923 Calvert, A.T., Moore, R.B., McGeehin, J.P., Rodrigues da Silva, A.M., 2006. Volcanic history  
924 and  $^{40}\text{Ar}/^{39}\text{Ar}$  geochronology of Terceira Island, Azores, Portugal. *J. Volcanol. Geoth. Res.*  
925 156, 103-115.

926 Camacho, A. G., Nunes, J.C., Ortiz, E., França, Z., Vieira, R., 2007. Gravimetric determination  
927 of an intrusive complex under the Island of Faial (Azores): some methodological  
928 improvements. *Geophys. J. Int.* 171, 478-494.

929 Carmichael, R. S., 1986. *Handbook of physical properties of rocks*. Boca Raton, Florida, CRC  
930 Press.

931 Catalão, J., Miranda, J.M., Lourenço, N., 2006. Deformation associated with the Faial  
932 (Capelinhos) 1956 eruption. Inferences from 1937-1997 geodetic measurements. *J. Volcan.  
933 and Geotherm. Res.* 155, 151-163.

934 Chiara, A., Speranza, F., Porreca, M., Pimentel, A., Caracciolo, F.A., Pacheco, J., 2014.  
935 Constraining chronology and time-space evolution of Holocene volcanic activity on the  
936 Capelo Peninsula (Faial Island, Azores): The paleomagnetic contribution. *GSA Bulletin* 126,  
937 1164–1180.

938 Chovelon, P., 1982. *Evolution volcanotectonique des îles de Faial et de Pico*. Ph.D. Thesis. Univ.  
939 Paris-Sud, Orsay, France, 186 pp.

940 Costa, A.C.G., Marques, F.O., Hildenbrand, A., Sibrant, A.L.R., Catita, C.M.S., 2014. Large-  
941 scale catastrophic flank collapses in a steep volcanic ridge: The Pico–Faial Ridge, Azores  
942 Triple Junction. *J. Volcanol. Geotherm. Res.* 272, 111–125.

943 Costa, A.C.G., Hildenbrand, A., Marques, F.O., Sibrant, A.L.R., Santos de Campos, A., 2015.  
944 Catastrophic flank collapses and slumping in Pico Island during the last 130 kyr (Pico-Faial

945 ridge, Azores Triple Junction). *Journal of Volcanology and Geothermal Research* 302, 33-46.

946 DeMets, C., Gordon, R.G., Argus, D.F., 2010. Geologically current plate motions. *Geo-phys. J.*  
947 *Int.* 181, 1–80.

948 Dong, D., Herring, T.A., King, R.W., 1998. Estimating regional deformation from a combination  
949 of space and terrestrial geodetic data. *J. Geod.* 72, 200–214.

950 Forjaz, V.H., 1966. Carta geológica do sistema vulcânico Faial-Pico-S. Jorge. Escala 1:200 000.  
951 In: Machado, F., Forjaz, V.H., (Eds.), *A actividade vulcânica na ilha do Faial (1957-67)*,  
952 1968, Comissão de Turismo da Horta, Portugal, 89 pp.

953 França, Z., 2000. Origem e evolução petrológica e geoquímica do vulcanismo da ilha do Pico.  
954 Açores. Ph.D. Thesis, Univ. Açores, Ponta Delgada, Portugal.

955 França, Z.T.M., Tassinari, C.C.G., Cruz, J.V., Aparicio, A.Y., Araújo, V., Rodrigues, N.R., 2006.  
956 Petrology, geochemistry and Sr-Nd-Pb isotopes of the volcanic rocks from Pico Island -  
957 Azores (Portugal). *J. Volcanol. Geotherm. Res.* 156 (1–2), 71–89.

958 Gente, P., Dymet, J., Maia, M., Goslin, L., 2003. Interaction between the Mid-Atlantic Ridge  
959 and the Azores hot spot during the last 85 Myr: emplacement and rifting of the hot spot-  
960 derived plateaus. *Geochem. Geophys. Geosyst.* 4, 8514, 10.1029/2003GC000527

961 Herring, T.A., King, R.W., McClusky, S.C., 2010. GLOBK Reference Manual Release 10.4.  
962 Department of Earth, Atmospheric, and Planetary Sciences, Massachusetts Institute of  
963 Technology, Cambridge.

964 Hildenbrand, A., Gillot, P.Y., Bonneville, A., 2006. Off-shore evidence for a huge landslide of the  
965 northern flank of Tahiti-Nui (French Polynesia). *Geochemistry Geophysics Geosystems* 7, 1-  
966 12.

967 Hildenbrand, A., Madureira, P., Marques, F.O., Cruz, I., Henry, B., Silva, P., 2008. Multi-stage  
968 evolution of a sub-aerial volcanic ridge over the last 1.3 Myr: S. Jorge Island, Azores Triple  
969 Junction. *Earth Planet. Sci. Lett.* 273 (3–4), 289–298.

970 Hildenbrand, A., Marques, F.O., Costa, A.C.G., Sibrant, A.L.R., Silva, P.M.F., Henry, B.,  
971 Miranda, J.M., Madureira, P., 2012a. Reconstructing the architectural evolution of volcanic  
972 islands from combined K/Ar, morphologic, tectonic, and magnetic data: the Faial Island  
973 example (Azores). *J. Volcanol. Geotherm. Res.* 241–242, 39–48.

974 Hildenbrand, A., Marques, F.O., Catalão, J., Catita, C.M.S., Costa, A.C.G., 2012b. Large-scale  
975 active slump of the southeastern flank of Pico Island, Azores. *Geology* 40, 939–942.  
976 <http://dx.doi.org/10.1130/G33303.1>.

977 Hildenbrand, A., Weis, D., Madureira, P., Marques, F.O., 2014. Recent plate re-organization at  
978 the Azores Triple Junction: Evidence from combined geochemical and geochronological data  
979 on Faial, S. Jorge and Terceira volcanic islands. *Lithos* 210-211, 27-39.

980 Hildenbrand, A., Marques, F.O., Catalão, J., 2018. Large-scale mass wasting on small volcanic  
981 islands revealed by the study of Flores Island (Azores). *Scientific Reports* 8, 13898.

982 Hübscher, C., Gohl, K., 2014. Reflection / Refraction Seismology. *Encyclopedia of Marine*  
983 *Geosciences*. DOI 10.1007/987-94-007-6644-0\_128-1

984 Hübscher, C., Beier, C., Al-Hseinat, M., et al., 2016. Azores Plateau – Cruise No. M113/1 –  
985 December 29, 2014 – January 22, 2015: Ponta Delgada (Portugal) – Ponta Delgada  
986 (Portugal). *METEOR-Berichte*, M113/1, 31 pp., DFG-Senatskommission für Ozeanographie,  
987 DOI:10.2312/cr\_m113\_1

988 Johnston, E.N., Sparks, R.S.J., Nomikou, P., Livanos, I., Carey, S., Phillips, J.C., Sigurdsson, H.,  
989 2015. Stratigraphic relations of Santorini's intracaldera fill and implications for the rate of  
990 post-caldera volcanism. *J. Geol. Soc. Lond.* 172, 323–335.

991 Karstens, J., Crutchley, G.J., Berndt, C., Talling, P.J., Watt, S.F.L., Hühnerbach, V., Le Friant,  
992 A., Lebas, E., Trofimovs, J., 2013. Emplacement of pyroclastic deposits offshore Montserrat:  
993 Insights from 3D seismic data. *Journal of Volcanology and Geothermal Research* 257, 1-11.

994 Krastel, S., Schmincke, H.U., Jacobs, C.L., Rihm, R., Le Bas, T.P., Alibés, B., 2001. Submarine

995 landslides around the Canary Islands. *J. Geophys. Res.* 106 (B3), 3977–3997.  
996 <http://dx.doi.org/10.1029/2000JB900413>.

997 Lange, R.A., Cashma, K.V., Navrotsky, A., 1994. Direct measurements of latent heat during  
998 crystallization and melting of a ugandite and an olivine basalt. *Contrib. Mineral. Petrol.* 118:  
999 169-181.

1000 Lourenço, N., 2007. Tectono-magmatic Processes at the Azores Triple Junction. Ph.D. Thesis,  
1001 Univ. Algarve, Faro, Portugal, 239 pp.

1002 Machado, F., Nascimento, J.M., Denis, A.F., 1959. Evolução Topográfica do cone Vulcânico  
1003 dos Capelinhos. *Le Volcanisme de l'île de Faial. Serv. Geol. Portugal, Mem., vol. 4, pp. 65–*  
1004 *71.*

1005 Machado, F., Parsons, W., Richards, A., Mulford, J.W., 1962. Capelinhos eruption of Fayal  
1006 Volcano, Azores, 1957–1958. *J. Geophys. Res.* 67 (9), 3519–3529.

1007 Madeira, J., 1998. Estudos de neotectónica nas ilhas do Faial, Pico e S. Jorge: Uma contribuição  
1008 para o conhecimento geodinâmico da junção tripla dos Açores. Ph.D. Thesis. Univ. Lisboa,  
1009 Portugal, 481 pp.

1010 Madeira, J., Monge Soares, A.M., Brum da Silveira, A., Serralheiro, A., 1995. Radiocarbon  
1011 dating recent volcanic activity on Faial island, Azores. *Radiocarbon* 37, 139-147.

1012 Madeira, J., Brum da Silveira, A., 2003. Active tectonics and first paleoseismological results in  
1013 Faial, Pico and S. Jorge islands (Azores, Portugal). *Ann. Geophys.* 46, 733–761.  
1014 <http://dx.doi.org/10.4401/ag-3453>.

1015 Madureira, P., Moreira, M., Mata, J., Allègre, C.J., 2005. Primitive helium and neon isotopes in  
1016 Terceira Island: constraints on the origin of the Azores archipelago. *Earth Planet. Sci. Lett.*  
1017 233, 429-440.

1018 Madureira, P., Mata, J., Mattielli, N., Queiroz, G., Silva, P., 2011. Mantle source heterogeneity,  
1019 magma generation and magmatic evolution at Terceira Island (Azores archipelago):

1020 constraints from elemental and isotopic (Sr, Nd, Hf, and Pb) data. *Lithos* 126, 402-418.

1021 Madureira, P., Moreira, M., Mata, J., Nunes, J.C., Gautheron, C., Lourenço, N., Carvalho, R.,  
1022 Abreu, M.P., 2014. Helium isotope systematics in the vicinity of the Azores triple junction:  
1023 constraints on the Azores geodynamics. *Chemical Geology*, 372, 62-71.

1024 Marques, F.O., Catalão, J.C., DeMets, C., Costa, A.C.G., Hildenbrand, A., 2013. GPS and  
1025 tectonic evidence for a diffuse plate boundary at the Azores Triple Junction. *Earth Planet. Sci.*  
1026 *Lett.* 381, 177–187. <http://dx.doi.org/10.1016/j.epsl.2013.08.051>.

1027 Marques, F.O., Catalão, J.C., DeMets, C., Costa, A.C.G., Hildenbrand, A., 2014a. Corrigendum  
1028 to " GPS and tectonic evidence for a diffuse plate boundary at the Azores Triple Junction"  
1029 [Earth Planet. Sci. Lett. 381 (2013) 177-187]. *Earth Planet. Sci. Lett.* 387, 1–3.

1030 Marques, F.O., Catalão, J., Hildenbrand, A., Costa, A.C.G., Dias, N.A., 2014b. The 1998 Faial  
1031 earthquake, Azores: Evidence for a transform fault associated with the Nubia-Eurasia plate  
1032 boundary?. *Tectonophysics* 633, 115-125. doi:10.1016/j.tecto.2014.06.024.

1033 Marques, F.O., Catalão, J., Hildenbrand, A., Madureira, P., 2015. Ground motion and tectonics in  
1034 the Terceira Island: Tectonomagmatic interactions in an oceanic rift (Terceira Rift, Azores  
1035 Triple Junction). *Tectonophysics* 651–652, 19–34.

1036 Marques, F.O., Hildenbrand, A., Hübscher, C., 2018. Evolution of a volcanic island on the  
1037 shoulder of an oceanic rift and geodynamic implications: S. Jorge Island on the Terceira Rift,  
1038 Azores Triple Junction. *Tectonophysics* 738-739, 41-50.

1039 Marques, F.O., Hildenbrand, A., Costa, A.C.G., Sibrant, A.L.R., 2020. The evolution of Santa  
1040 Maria Island in the context of the Azores Triple Junction. *Bulletin of Volcanology* 82, 39  
1041 <https://doi.org/10.1007/s00445-020-01378-4>.

1042 Mendes, V.B., Madeira, J., Brum da Silveira, A., Trota, A., Elosegui, P., Pagarete, J., 2013.  
1043 Present-day deformation in São Jorge Island, Azores, from episodic GPS measurements  
1044 (2001–2011). *Adv. Space Res.* 51, 1581–1592.

1045 Métrich, N., Zanon, V., Créon, L., Hildenbrand, A., Moreira, M., Marques, F.O., 2014. Is the  
1046 “Azores hotspot” a wetspot? Insights from the geochemistry of fluid and melt inclusions in  
1047 olivine of Pico basalts. *Journal of Petrology* 55, 377-393.

1048 Miranda, J.M., Luis, J.F., Lourenço, N., Goslin, J., 2014. Distributed deformation close to the  
1049 Azores Triple "Point". *Mar. Geol.* 355, 27–35.

1050 Moreira, M., Doucelance, R., Dupré, B., Allègre, C.J., 1999. Helium and lead isotope  
1051 geochemistry in the Azores. *Earth Planet. Sci. Lett.* 169, 189-205.

1052 Navarro, A., Catalão, J., Miranda, J. M., Fernandes, R.M., 2003. Estimation of the Terceira  
1053 Island (Azores) main strain rates from GPS data. *Earth, Planets and Space* 55, 637-642.

1054 Nunes, J.C., 1999. A actividade vulcânica na ilha do Pico do Plistocénico Superior ao  
1055 Holocénico: Mecanismo eruptivo e hazard vulcânico. Ph.D. Thesis. Univ. Açores, Ponta  
1056 Delgada, Portugal, 356 pp.(available at: <http://www.jcnunes.uac.pt/principal.htm>)

1057 Nunes, J.C., Camacho, A., França, Z., Montesinos, F.G., Alves, M., Vieira, R., Velez, E., Ortiz,  
1058 E., 2006. Gravity anomalies and crustal signature of volcano-tectonic structures of Pico Island  
1059 (Azores). *J. Volcanol. Geotherm. Res.* 156, 55–70.

1060 Pacheco, J.M., 2001. Processos associados ao desenvolvimento de erupções vulcânicas  
1061 hidromagmáticas explosivas na ilha do Faial e sua interpretação numa perspectiva de  
1062 avaliação do hazard e minimização do risco. Ph.D. thesis, Azores University, Ponta Delgada,  
1063 S. Miguel Island, Azores, Portugal. 330 pp.

1064 Parman, S.W., 2007. Helium isotopic evidence for episodic mantle melting and crustal growth.  
1065 *Nature* 446, 900-904.

1066 Pollet, N., Schneider, J.-L.M., 2004. Dynamic disintegration processes accompanying transport  
1067 of Holocene Flims sturzstrom (Swiss Alps). *Earth and Planetary Science Letters* 221, 433-  
1068 448.

1069 Prytulak, J., Elliott, T., 2009. Determining melt productivity of mantle sources from  $^{238}\text{U}$ - $^{230}\text{Th}$

1070 and  $^{235}\text{U}$ – $^{231}\text{Pa}$  disequilibria; an example from Pico Island, Azores. *Geochimica et*  
1071 *Cosmochimica Acta* 73, 2103-2122.

1072 Ramalho, R.S., Helffrich, G., Madeira, J., Cosca, M., Thomas, C., Quartau, R., Hipólito, A.,  
1073 Rovere, A., Hearty, P.J., Ávila, S.P., 2017. Emergence and evolution of Santa Maria Island  
1074 (Azores): the conundrum of uplifted islands revisited. *Geol. Soc. Am. Bull* 129, 372–390.

1075 Romer, R., Beier, C., Haase, K.M., Hübscher, C., 2018. Correlated changes between volcanic  
1076 structures and magma composition in the Faial volcanic system, Azores. *Frontiers in Earth*  
1077 *Science*, Vol 6. DOI=10.3389/feart.2018.00078.

1078 Saastamoinen, J., 1972. Contributions to the theory of atmospheric refraction: part I. *Bull. Géod.*  
1079 105, 279–298.

1080 Saastamoinen, J., 1973. Contribution to the Theory of Atmospheric Refraction: part II. *Bulletin*  
1081 *Géodésique* 107, 13-34.

1082 Schilling, J.-G., Bergeron, M.B., Evans, R., 1980. Halogens in the mantle beneath the North  
1083 Atlantic. *Philosophical Transactions of the Royal Society of London. Series A, Mathematical*  
1084 *and Physical Sciences* 297, 147–178.

1085 Schmidt, C., Hensen, C., Hübscher, C., Wallmann, K., Liebetrau, V., Schmidt, M., Kutterolf, S.,  
1086 Hansteen, T.H., 2020. Geochemical characterization of deep-sea sediments on the Azores  
1087 Plateau – From diagenesis to hydrothermal activity. *Marine Geology* 429,  
1088 <https://doi.org/10.1016/j.margeo.2020.106291>

1089 Schön, J.H., 2004. Physical properties of rocks. *Handbook of Geophysical Exploration*.  
1090 Amsterdam, NL, Elsevier.

1091 Serralheiro, A., Matos Alves, C.A., Forjaz, V.H., and Rodrigues, B., 1989. *Carta Vulcanológica*  
1092 *dos Açores, Ilha do Faial*: Ed. Serviço Regional de Protecção Civil, Universidade dos Açores  
1093 and Centro de Vulcanologia INIC: Instituto Nacional de Investigação Científica, 4 sheets,  
1094 scale 1:15,000.

1095 Sibrant, A.L.R., Marques, F.O., Hildenbrand, A., 2014. Construction and destruction of a  
1096 volcanic island developed inside an oceanic rift: Graciosa Island, Terceira Rift, Azores. *J.*  
1097 *Volcanol. Geotherm. Res.* 284, 32-45.

1098 Sibrant, A.L.R., Hildenbrand, A., Marques, F.O., Costa, A.C.G., 2015a. Volcano-tectonic  
1099 evolution of the Santa Maria Island (Azores): implications for paleostress evolution at the  
1100 western Eurasia-Nubia plate boundary. *J. Volcanol. Geotherm. Res.* 291, 49–62.

1101 Sibrant, A.L.R., Hildenbrand, A., Marques, F.O., Weiss, B., Boulesteix, T., Hübscher, C.,  
1102 Lüdmann, T., Costa, A.C.G., Catalão, 2015b. Morpho-structural evolution of a volcanic  
1103 island developed inside an active oceanic rift: S. Miguel Island (Terceira Rift, Azores).  
1104 *Journal of Volcanology and Geothermal Research* 301, 90-106.

1105 Sibrant, A.L.R., Marques, F.O., Hildenbrand, A., Boulesteix, T., Costa, A.C.G., Catalão, J.,  
1106 2016. Deformation in a hyper-slow oceanic rift: insights from the tectonics of the S. Miguel  
1107 Island (Terceira Rift, Azores). *Tectonics* 35. <http://dx.doi.org/10.1002/2015TC003886>.

1108 Silva, P., Henry, B., Marques, F.O., Hildenbrand, A., Lopes, A., Madureira, P., Madeira, J.,  
1109 Nunes, J., Roxerová, Z., 2018. Volcano-tectonic evolution of a linear volcanic ridge (Pico-  
1110 Faial Ridge, Azores Triple Junction) assessed by paleomagnetic studies. *Journal of*  
1111 *Volcanology and Geothermal Research* 352, 78-91.

1112 Silveira, G., Stutzmann, E., Davaille, A., Montagner, J. P., Mendes-Victor, L., Sebai, A. 2006.  
1113 Azores hotspot signature in the upper mantle. *Journal of Volcanology and Geothermal*  
1114 *Research* 156, 23-34.

1115 Tripanera, D., Porreca, M., Ruch, J., Pimentel, A., Acocella, V., Pacheco, J., Salvatore, M.,  
1116 2013. Relationships between tectonics and magmatism in a transtensive/transform setting: An  
1117 example from Faial Island (Azores, Portugal). *Geological Society of America Bulletin* 126 (1-  
1118 2), 164-181.

1119 Turcotte, D., Schubert, G., 2014. *Geodynamics*. Cambridge University Press, 3<sup>rd</sup> edition,

1120 Cambridge, UK, 636 pp.

1121 Weiß, B., Hübscher, C., Lüdmann, T., 2015a. The tectonic evolution of the southeastern Terceira  
1122 Rift/São Miguel region (Azores). *Tectonophysics* 654, 75-95.

1123 Weiß, B., Hübscher, C., Wolf, D., Lüdmann, T., 2015b. Submarine explosive volcanism in the  
1124 southeastern Terceira Rift / São Miguel Region (Azores). *Journal of Volcanology and*  
1125 *Geothermal Research* 303, 79-91.

1126 Weiß, B., Hübscher, C., Lüdmann, T., Serra, N., 2016. Submarine sedimentation processes in the  
1127 southeastern Terceira Rift / São Miguel region (Azores). *Marine Geology* 374, 42-58.

1128 Woodhall, D., 1974. Geology and volcanic history of Pico Island Volcano, Azores. *Nature* 248,  
1129 663–665.

1130 Yang, T., Shen, Y., van der Lee, S., Solomon, S.C., Hung, S.-H. 2006. Upper mantle structure  
1131 beneath the Azores hotspot from finite-frequency seismic tomography. *Earth and Planetary*  
1132 *Science Letters* 250, 11-26.

1133 Zanon, V., Frezzotti, M. L., 2013. Magma storage and ascent conditions beneath Pico and Faial  
1134 islands (Azores Islands): 1. A study on fluid inclusions. *Geochem. Geophys. Geosyst.* 14,  
1135 3494–3514.

1136 Zanon, V., Kueppers, U., Pacheco, J., Cruz, I., 2013. Volcanism from fissure zones and the  
1137 Caldeira central volcano at Faial Island, Azores archipelago: geochemical processes in  
1138 multiple feeding systems. *Geological Magazine* 150, 536-555.

1139 Zanon, V., Pimentel, A., Auxerre, M., Marchini, G., Stuart, F.M., 2020. Unravelling the magma  
1140 feeding system of a young basaltic oceanic volcano. *Lithos*, 352-353, 105325, doi:  
1141 10.1016/j.lithos.2019.105325.

1142 Zbyszewski, G., da Veiga Ferreira, O., 1959. Rapport de la Deuxième mission Géologique. Le  
1143 Volcanisme de l'île de Faial. *Serv. Geol. Portugal, Mem.*, vol. 4, pp. 29–55.

1144 Zbyszewski, G., Ribeiro Ferreira, C., Veiga Ferreira, O., Torre de Assunção, C., 1963. Notícia

- 1145 explicativa da Folha "B" da Ilha do Pico (Açores). Carta Geológica de Portugal na escala 1/50
- 1146 000. Serviços Geológicos de Portugal. Lisbon, Portugal. 21 pp.
- 1147